Heat Transfer Research 52(10):19–45 (2021)

NUMERICAL AND EXPERIMENTAL ANALYSIS OF LONGITUDINAL TUBULAR SOLAR AIR HEATERS MADE FROM PLASTIC AND METAL WASTE MATERIALS

Ataollah Khanlari,[1,] Adnan Sözen,[2] Azim Doğuş Tuncer,[3,4] Faraz Afshari,[5] Emine Yağız Gürbüz,[4,6] & Yaşar Can Bilge[3]*

[1]*Mechanical Engineering, University of Turkish Aeronautical Association, Ankara, Turkey*

[2]*Energy Systems Engineering, Gazi University, Ankara, Turkey*

[3]*Energy Systems Engineering, Burdur Mehmet Akif Ersoy University, Burdur, Turkey*

[4]*Natural and Applied Science Institute, Gazi University, Ankara, Turkey*

[5]*Mechanical Engineering, Erzurum Technical University, Turkey*

[6]*Energy Systems Engineering, Muğla Sıtkı Koçman University, Muğla, Turkey*

*Address all correspondence to: Ataollah Khanlari, Mechanical Engineering, University of Turkish Aeronautical Association, Ankara, Turkey, E-mail: ata_khanlari@yahoo.com

Original Manuscript Submitted: 2/27/2021; Final Draft Received: 4/27/2021

Recycling and reusing waste materials not only reduces environmental pollution but also contributes to the reduction of health problems and economic gain. In this study, plastic and metal materials reused in fabricating solar air heaters (SAHs) are considered. Accordingly, two tubular solar air heaters have been designed, fabricated, and experimented. The major objective of this work is to demonstrate the importance of utilizing waste materials in renewable energy-based technologies and their applicability in thermal energy production. In the first step of the analysis, the applicability of tubular-type SAHs has been studied numerically. The experiments have been conducted at two tilt angles including 90^o and 32^o and also at three flow rates including 0.012, 0.010, and 0.008 kg/s. The experimental findings showed that the efficiency of metal SAH and plastic SAH varied in the range of 36.33–50.96% and 31.60–47.06%, respectively. Also, enviro-economic costs for metal and plastic SAH were achieved as 8.02 and 7.55 $/year. Besides, the experimental results were predicted with ANN and SVM algorithms. The prediction success of the algorithms is discussed with four metrics (R^2, MAPE, RMSE, and MBE). The outcomes clearly demonstrate the successful application of this simple and cost-effective tubular-type SAH manufactured from waste materials.

KEY WORDS: *solar air heater, waste material, reusing, enviro-economic analysis, modeling*

1. INTRODUCTION

In the modern world, waste management is a crucial issue for a sustainable environment because of the growing world population. Industrialization, rapid urbanization, and changing consumption habits are the main factors which affect the environment negatively (Minelgaite and Liobikiene, 2019; Singh, 2019). It can be said that increasing industrial production due to rising demand and consequently an increase in the amount of waste has a significant share of environmental pollution. Increasing the amount and type of waste materials and consequently, the environmental effects of them have reached dangerous levels. Changing consumption habits have also affected the characteristics of solid wastes. The amount of solid waste varies according to the general socio-economic structure of the countries. However, depending on the social characteristics of the cities within the borders of the same

NOMENCLATURE

A	area, m^2
AC	annual cost, $
c_p	specific heat, kJ/kg·K
COP	coefficient of performance
C_{cost}	capital cost, $
$C_{recoveryfactor}$	capital recovery factor
C_u	useful energy cost, $/kWh
CDA	CO_2 reduction annually, ton CO_2/year
CFD	computational fluid dynamics
CP_{CO2}	mean international price of carbon, 14.5 $/t$CO_2$
D_{hyd}	hydraulic diameter, m
E_{useful}	daily useful energy, kWh
$E_{collector}$	energy produced annually by the collector
F_R	heat removal factor
FCS	annual revenue of fuel consumption saving
h	convective heat transfer coefficient, $W/m^2 \cdot K$
I	solar radiation, W/m^2
k	thermal conductivity, W/m·K
$\dot{m}$	mass flow rate, kg/s
MAPE	mean absolute percentage error
MBE	mean bias error
Nu	Nusselt number
p	pressure, Pa
$\dot{Q}_\rho$	reflected energy from absorber, W
$\dot{Q}_{loss}$	heat losses, W
$\dot{Q}_u$	useful heat, W
R^2	coefficient of determination
Re	Reynolds number
RMSE	root-mean-square error
SPBP	simple payback period
SV	salvage value, $
T	temperature, K
U_{loss}	heat loss coefficient, $W/m^2 \cdot K$
V	air velocity, m/s
$\dot{V}$	volumetric flow rate, m^3/s
$\dot{W}_f$	fan power, W
W_R	total uncertainty, %
Z_{CO2}	enviro-economic cost, $/year

Greek Symbols

η_t	thermal efficiency, %
μ	dynamic viscosity, Pa·s
ρ	density, kg/m^3
$\tau\alpha$	transmittance–absorptance effective product
ϕ_{CO2}	CO_2 saved annually, ton/year
ψ_{CO2}	mean CO_2 equivalent intensity for electricity generation, 0.523 kg CO_2/kWh

Subscripts

a	air
aa	ambient air
as	absorber surface
in	inlet
ou	outlet

country and the lifestyle of those cities, their consumption habits differ (Fidelis et al., 2020). Sustainable development and waste management concepts are frequently encountered in waste management researches. The reason for this can be explained by evaluating environmental and sustainable development issues from different perspectives. The variety of environmental problems and limited natural resources in the world make it essential to find out appropriate solutions and sustainable development (Fuldauer et al., 2019; Pujara et al., 2020; Zhou et al., 2019).

Plastic materials are important commercial materials that are used in many fields and possess some advantages. They have low weight, are inexpensive and easy to process. However, a big part of plastics are used only once and they are not easily disposable, which makes them an important environmental problem worldwide. Approximately 7% of the plastic consumption was composed of polyethylene terephthalate (PET) worldwide, reaching about 19 million tons in 2015 (Taniguchi et al., 2019). Some researchers present that 62% of generated bottles are made of PET, and PET bottles account for nearly 2/3 of all bottles collected for reusing and recycling. Also, recycling rate for PET plastic bottles raised from 28.4% in 2016 to about 30% in 2017 (Zhang et al., 2020). However, the collection and recycling of secondary PET does not exceed 50% worldwide (Aizenshtein, 2016). Recycled and reused PET offers important positive environmental impacts compared with virgin PET. Nowadays, the world is paying attention to reusing and recycling with the intention of decreasing PET waste and utilizing resources rationally (Shen et al., 2010). The most important way to reduce plastic waste is recycling and reuse of plastic (Gardas et al., 2019). Plastic wastes can be transformed into a new raw material through different physical or chemical processes. Recycling and reusing plastic wastes not only decreases environmental pollution but also contributes to the reduction of health problems and economic gain.

Similarly, metal wastes can be recycled or reused by various processes and could be utilized in different applications. In recent years, various studies were performed which investigated recycling and reusing e-wastes (Tansel, 2017; Shaikh et al., 2020; Gunarathne et al., 2020) and also construction metal wastes (Galvin et al., 2012; Yu et al., 2018; Hadavand and Imaninasab, 2019).

The effectiveness of environmental sustainability depends on giving priority to the utilization of clean energy sources. Solar energy as a renewable and clean energy source has a great potential to be utilized in different fields (Hosseini et al., 2018; Lamnatou et al., 2019).

Thermal energy production from solar energy is extensively used in many regions around the world. Solar heating systems are generally divided into solar air and solar water heaters. Solar heaters (SH) are usually utilized in space heating, drying applications, greenhouse air conditioning system, etc. (Kaya et al., 2019; Gürel, 2016). A big part of the energy is utilized in heating applications in residential buildings. Heating and cooling (mainly heating) accounted for almost 50% of the overall energy demand in the European countries in 2017 (Stolarski et al., 2020). In cold seasons, space heating consumes large amounts of energy. As is known, some buildings like sport complexes, shopping centers, university buildings, and residential buildings need fresh and heated air in cold months of the year. Also, drying appliances providing hot air need large amounts of energy. There are some solar air heating systems that are used for hot air generation in various applications. Gao et al. (2020) developed a transpiration solar heating system to provide heated air for buildings. Wang et al. (2017) analyzed a transpiration SH and indicated the potential of the developed system in supplying fresh and hot air. Charvat et al. (2019) manufactured solar air heaters and utilized phase change material to provide hot air at night. Raj et al. (2019) developed a double-pass SH to be utilized in different applications.

Researchers have investigated various solar heaters (SH) form different points of view. In general, the performance of solar heaters was improved by extending the heat transfer surface area of the absorber. In this regard, some obstacles like fins and baffles could be integrated into the absorber. In addition, some researchers used waste materials in manufacturing SHs. Ozgen et al. (2009) utilized aluminum cans in manufacturing a double-flow solar heater. They indicated that integrating aluminum cans on the absorber surface increased the effectiveness of solar heater notably. In another study, Kishk et al. (2019) manufactured a solar heater by using aluminum cans in drying applications. They attained the efficiency in the range of 25–63% for the developed heater. Murali et al. (2020a) manufactured a solar heater utilizing aluminum cans filled with aluminum scraps and pebble stones for energy storage. Their results showed that pebble stones as storage material exhibited better performance than aluminum scraps. In another study, Murali et al. (2020b) experimentally analyzed the effect of using aluminum cans in a SH with fins and without fins. They stated that in a finned heater maximum thermal efficiency reached 69.47% and in the heater without fins it reached 65.98%. In addition to the experimental studies, there are some researches where the CFD method is employed to investigate different solar energy systems. Nidhul et al. (2020) used the CFD approach to analyze roughened SH with half-cylindrical walls to specify its thermal performance. Craig et al. (2020) utilized the CFD method to investigate a tubular type cavity dish receiver at different inclination angles to specify the impacts of various factors. Kong et al. (2020) numerically investigated the optimal inclination angle for a roof-

placed solar chimney to be used for ventilation. Moghimi et al. (2021) experimentally and numerically analyzed a household solar drying system to be used in drying agricultural crops and showed the importance of the CFD approach in investigating solar energy systems.

As is known, using a tubular-type absorber could enhance the overall efficiency by supplying perpendicular angle between the absorber surface and incoming sun rays. In the last years, some researchers developed tubular-type SHs and indicated that utilizing a tubular-type SH can significantly enhance the thermal performance (Abo-Elfadl et al., 2020; Sözen et al., 2020; Hassan et al., 2020; Afshari et al., 2020). An analysis of available researches in the field of solar thermal applications showed that there are limited studies available where waste materials are used in manufacturing solar energy systems. In this study, plastic and galvanized sheet metal materials are reused for fabrication of solar air heaters. Accordingly, two tubular solar air heaters (TSH) have been designed, fabricated, and experimented. In contrast to the available studies where waste materials are reused as additional parts of the heaters especially in the absorber plate, in the solar heaters investigated in this study the main part of the heaters (excluding fan and sealing material) has been manufactured from the reused waste materials. The major objective of the study is to demonstrate the significance of utilizing waste materials in renewable energy-based technologies and their applicability in thermal energy production. Another important point of the study is both to predict the experimental results with the frequently used machine learning algorithms, and to make a comparison between the algorithms. Accordingly, Fig. 1 illustrates the major structure of the present work.

2. MATERIALS AND METHODS

2.1 CFD Study

In the present study, it is aimed to develop tubular-type solar air heaters by using plastic and sheet metal materials. In daily life, plastic bottles are extensively used which are not easily disposable. So, recycling and reutilizing these waste materials can help the environment. The upper and lower parts of the plastic bottles could be cut and the bottles acquired a shape of tubes. In this section, plastic and metal tubes have been analyzed numerically to investigate their applicability as tubular-type solar heaters. Plastic bottles of 1.5-L and 5-L volume are widely used for water and beverage packaging. In this context, two tubes with 90-mm and 150-mm diameters have been selected for analysis as TSHs (Fig. 2). Sheet metal and plastic materials' properties have been defined in the materials section in the Fluent software. In the numerical analysis part, the velocity of flowing air has been defined as 1.8,

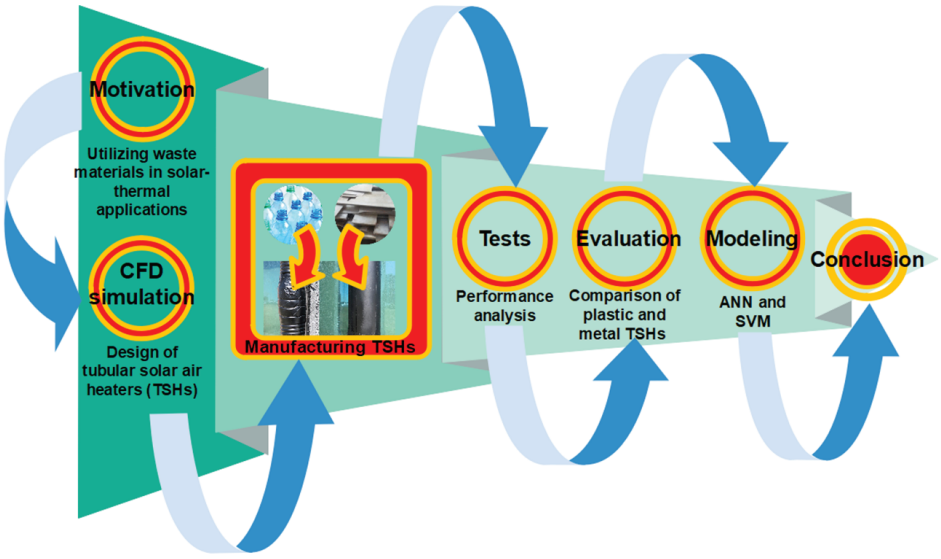

FIG. 1: Major structure of the present work

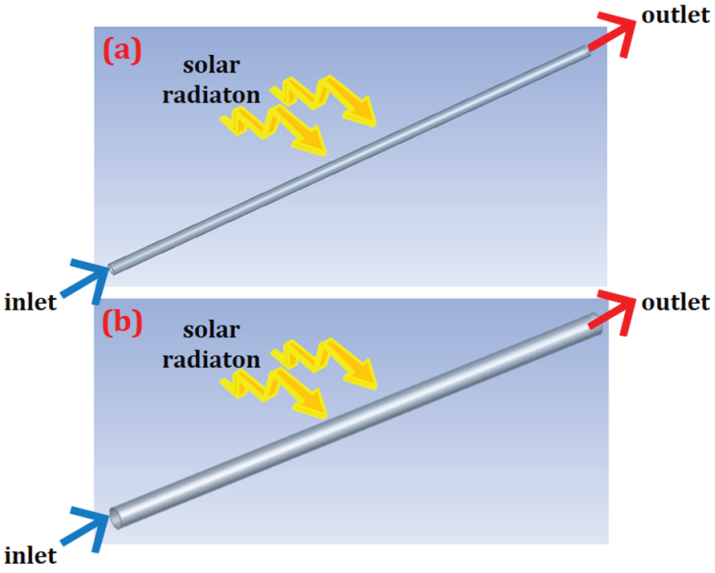

FIG. 2: Geometry of TSHs: a) with 90-mm diameter, b) with 150-mm diameter

2.4, and 3 m/s. These velocity values correspond to 0.008, 0.010, and 0.012 kg/s air flow rates. It must be said that this velocity value corresponds to the turbulent flow regime. Therefore, in this work, a turbulent flow has been simulated and investigated for both TSHs. The governing equations including momentum, continuity, and energy equations that are used in the numerical investigation section are as follows (Karagoz et al., 2017):

continuity

$$\frac{\partial \rho}{\partial t} + \frac{\partial}{\partial x_i}\left(\rho v_i\right) = 0\,, \tag{1}$$

momentum

$$\frac{\partial}{\partial x_j}\left(\rho v_i v_j\right) = \frac{-\partial P}{\partial x_i} + \frac{\partial}{\partial x_j}\left[\mu\left(\frac{\partial v_i}{\partial x_j} + \frac{\partial v_j}{\partial x_i}\right) - \frac{2}{3}\,\mu\,\frac{\partial v_k}{\partial x_k}\,\delta_{ij}\right], \tag{2}$$

energy

$$\frac{\partial}{\partial t}\left(\rho e\right) + \frac{\partial}{\partial x_j}\left(\rho v_j c_p T - k\,\frac{\partial T}{\partial x_j}\right) = u_j\,\frac{\partial p}{\partial x_j} + \left[\mu\left(\left(\frac{\partial v_i}{\partial x_j} + \frac{\partial v_j}{\partial v_i}\right) - \frac{2}{3}\,\frac{\partial v_k}{\partial x_k}\,\delta_{ij}\right)\right]. \tag{3}$$

In the simulation part of the present work, different viscous models have been examined and the RNG k–ε model has been applied in all analyses. The RNG k–ε turbulence model is a convenient model for extensive engineering applications. In the previous researches, different options of the k–ε turbulence model were used for simulating different types of solar heaters and their findings exhibited the precision of this model (Khanlari et al., 2020; Tuncer et al., 2020; Afshari et al., 2020). In this regard, in turbulent flow modeling of TSHs, the RNG submodel of the k–ε turbulence model has been adopted in numerical calculations. Moreover, the enhanced wall function has been chosen to achieve more reliable findings in the domain near the tube wall. The related k–ε model equations are as follows (Karagoz et al., 2017):

$$\frac{\partial}{\partial t}\left(\rho k\right) + \frac{\partial}{\partial x_i}\left(\rho k v_i\right) = \frac{\partial}{\partial x_j}\left[\left(\frac{\mu + \mu_t}{\sigma_k}\right)\frac{\partial k}{\partial x_j}\right] + \mu_t\left(\frac{\partial v_i}{\partial x_j} + \frac{\partial v_j}{\partial v_i}\right)\frac{\partial v_i}{\partial x_j} - \rho\varepsilon\,, \tag{4}$$

$$\frac{\partial}{\partial t}(\rho\varepsilon)+\frac{\partial}{\partial x_i}(\rho\varepsilon v_i)=\frac{\partial}{\partial x_j}\left[\left(\frac{\mu+\mu_t}{\sigma_\varepsilon}\right)\frac{\partial \delta}{\partial x_j}\right]+C_{1\varepsilon}\frac{\varepsilon}{k}\mu_t\left(\frac{\partial v_i}{\partial v_j}+\frac{\partial v_j}{\partial v_i}\right)\frac{\partial v_i}{\partial v_j}-C_{2\varepsilon}\rho\frac{\varepsilon^2}{k}-\alpha\rho\frac{\varepsilon^2}{k}, \quad (5)$$

$$\mu_t=\rho C_\mu\frac{k^2}{\varepsilon}. \quad (6)$$

In the numerical analysis of TSHs, thermophysical properties of fluid were assumed to be constant and the effect of gravity was neglected. The tube inlet was set as velocity inlet and inlet temperature of the fluid was kept constant. The above-mentioned equations were discretized by the finite volume technique utilizing the semi-implicit method for pressure-linked equations (SIMPLE) pressure–velocity coupling solution. It is better to state that the convergence criterion was selected as 10^{-6} for the flow equation and 10^{-8} for the energy equation to obtain more accurate outcomes. The inlet air temperature was set to 30°C in order to correspond to average ambient temperature in August in the test region.

Mesh generation of analyzing domain is an important factor that has a significant effect on numerical results accuracy. In this regard, generated meshes with 53,656, 270,896, 480,000, 644,652, and 878,447 elements for the tube with 90-mm diameter have been tested. In addition, generated meshes with 178,500, 342,548, 577,393, 817,000, and 1,040,094 elements for the tube with 150-mm diameter have been examined. Figure 3 represents change in TSHs outlet temperature via mesh element number. The initial findings of the numerical study presented that the outlet temperature as the main parameter does not change with further increase in the number of mesh elements and keeps constant. Therefore, 878,447 and 1,040,094 mesh elements were selected for tubes with 90-mm and 150-mm diameter, respectively. Skewness of mesh is a crucial factor that demonstrates the quality of generated mesh. The highest and average skewness values in the generated mesh for TSH with a 90-mm diameter are 0.66 and 0.14, respectively. Moreover, maximum and mean skewness values in the generated mesh for TSH with a 150-mm diameter are 0.69 and 0.18, respectively. It must be said that in this research, steady-state heat flux was used as solar radiation boundary condition. In addition, half area of tubular SHs total surface area was selected to apply heat flux.

2.2 Experimental Setup

In this research, two tubular SHs have been fabricated from waste materials considering numerical simulation results. The first tubular heater has been made from plastic bottles (PTSH) with 1.5-L capacity. The upper and lower parts of the bottles were cut and the bottles were formed as tubes. Sixteen plastic bottles with 90-mm diameter

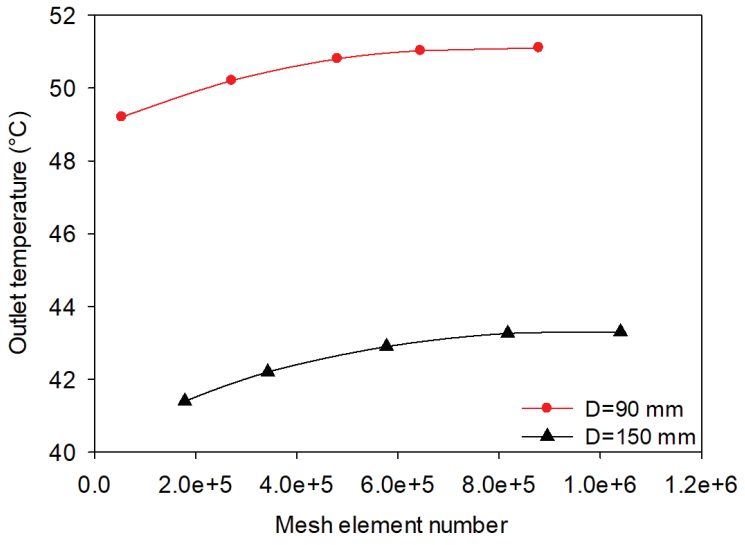

FIG. 3: Change in TSHs outlet temperature via mesh element number

FIG. 4: Manufactured tubular solar heaters: a) wall-mounted (90^o), b) angular placement (32^o)

and 200-mm length have been joined to each other and a 4-m-long single tube was obtained. The second tubular heater has been made from scrap sheet metal (MTSH). In this context, 5 sheet metal tubes with 1-mm thickness have been joined to obtain a 4-m-long tube with 90-mm diameter. The metal used for MTSH is galvanized sheet. Galvanized scrap sheet metal with the same thickness has been provided from heating stove factory, cold-rolled and spot welded to obtain smooth tubes. The density and thermal conductivity of galvanized sheet metal are 7.85 g/cm^3 and 24 W/m·K, respectively. Also, density and thermal conductivity of PET are 1.40 g/cm^3 and 0.4 W/m·K, respectively. Moreover, to supply air flow a fan with 40-W power has been mounted at the inlet of each heater. The liquid hermetic was used to obtain sealing in heaters. Both tubular-type heaters have been painted with matte black paint. In addition, platforms with proper tilt angles for the test region have been manufactured. In wall mounted SHs, in order to prevent contact between a tubular SH and a building wall, a thin slice (thickness: 20 mm, width: 40 mm) of extruded polystyrene (XPS) has been placed between the tube and the wall. The manufactured tubular heaters are presented in Fig. 4.

2.3 Experimental Procedure

The performance experiments of tubular heaters have been performed in Burdur province of Turkey. The experiments have been performed between 09:00–17:00. The manufactured tubular solar heaters have been experimented at two tilt angles and three air flow rates. Table 1 presents test parameters in detail. PTSH and MTSH heaters have been tested simultaneously to make a reliable comparison and totally 6 experiments have been performed. It should be indicated that the experiments have been conducted at two tilt angles including 90^o (wall-mounted) and 32^o (angular placement) as seen in Fig. 4. The tilt angle of 32^o has been selected by considering the optimal yearly tilt angle of the test region for conventional solar heaters (Tuncer et al., 2020). Also, the tilt angle of 90^o (wall-mounted) has been tested to determine the behavior of TSH regarding wall-type solar heater. These two angular placements have been tested at three mass flow rates. In other words, the experimental process of this study

TABLE 1: Controlled parameters in the current study

Experiment No.	Tilt Angle, deg	Mass Flow Rate, kg/s
1	90	0.012
2	90	0.010
3	90	0.008
4	32	0.012
5	32	0.010
6	32	0.008

contains six test days. In the experimental part of this study, it was aimed to examine the thermal performance of the TSHs which were made from metal and plastic materials. The tests have been carried out in consecutive days in August. In the experiments a solarimeter (Brand/model: CEM/LA-1017, accuracy: ± 10 W/m^2, range: 0–1999 W/m^2), thermocouples (Brand/model: Elimko/K Type, accuracy: ± 0.5^{o}C, range: (–200)–(+1200)^{o}C), a data logger (Brand/model: Testo/176T4, accuracy: ± 0.3^{o}C, range: (–195)–(+1200)^{o}C), an anemometer (Brand/model: Lutron/AM4202, accuracy: ± 2%, range: 0.4–30 m/s), and a multimeter (Brand/model: TROTEC BE47, accuracy: ± 1%/± 2%, range: 0.001–600 V/0.01–10 A) have been used to measure solar radiation, temperature, data collecting, air flow rate, and voltage–current, respectively.

In this study, TSHs have been developed with the aim of generating heated air to be utilized in different applications like space heating and drying. The proposed solar air heaters have been tested in August to determine the highest outlet temperature. This fact can show the potential utilization of the developed TSHs in drying applications.

2.4 Prediction Methodologies

In this research, frequently applied machine learning algorithms—artificial neural network (ANN), and support vector machine (SVM)—are used to predict system responses. Both algorithms are run on RapidMiner Studio Version 9.6. The grid-search technique is a frequently used optimization technique for the model parameters of machine learning algortihms (Ağbulut et al., 2021), and this technique is also used to tune the parameters in the present paper. In both algorithms, the dataset was randomly split as the shuffled sampling mode. Then it was divided into two parts as training data and testing data. Seventy percent of all dataset is used to train the algorithms, and then the remaining part (30%) is used to test and observe the prediction success of the algorithms. Short details about the ANN and SVM algorithms are given below.

In the field of machine learning, the ANN algorithm is considered as the most widely utilized approach for optimization, simulation, clustering, pattern detection, prediction, and solution of nonlinear function. Moreover, ANN behaves like a human brain and its structure is similar to a human nervous system (Gürel et al., 2020; Kırbaş et al., 2019).

Basically, ANN performs in two steps: first learning and second storing the data sets in weights. As is known, an ANN model basically includes three layers. These are input, hidden, and output layers, respectively (Ceylan et al., 2017). The ANN tool is extensively utilized for estimation of data that is mainly based on the parameters used in the input layer, the structure of neural model and learning process. For the process of learning different algorithms are used, which decreases the errors among actual and predicted values by updating weights and biases. The main advantages of the ANN approach are the ability to solve a complex problem that is not solved by other conventional methods and very fast processing speed. In all three developed ANN models, the numbers of input and output layers are 6 and 1, respectively. The hidden layer for thermal efficiency, gained energy, and COP models contains 9, 15, and 9 neurons, respectively. The architecture of the developed ANN models is given in Fig. 5 Material, tilt angle, mass flow rate, hour, ambient temperature, and solar radiation values were selected as input neuron. The developed models differ in the quantity of neurons in the hidden layer. As the learning algorithm, a feed-forward neural network was utilized and trained by a backpropagation algorithm (multilayer perceptron) in the present work.

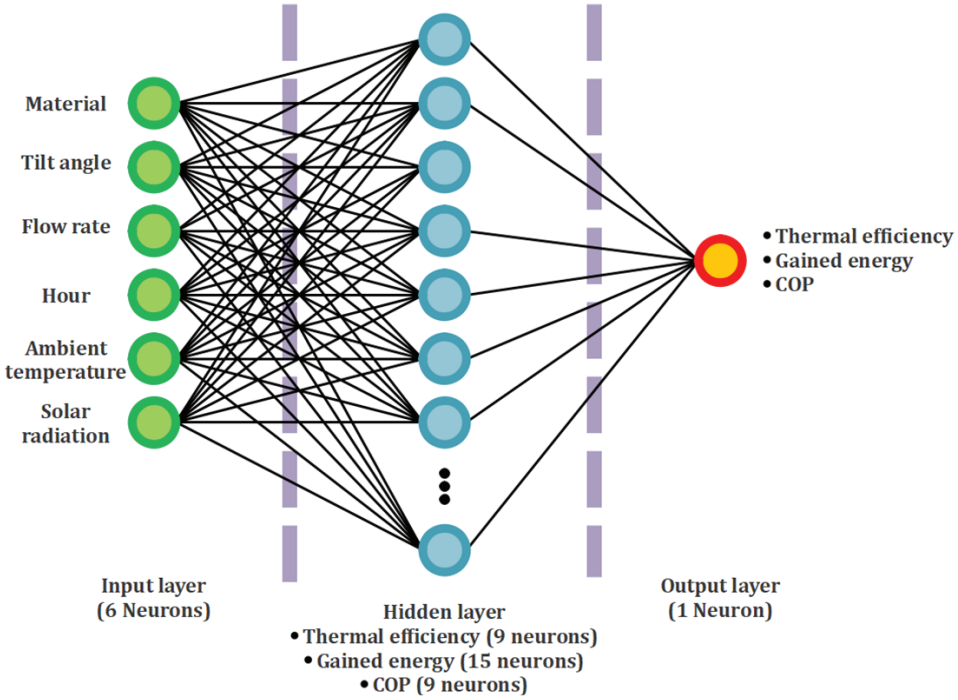

FIG. 5: Architecture of the developed ANN models

The support vector machine (SVM) approach is an accurate machine learning technique for both classification and regression (Burges, 1998). It has very robust principles and is a very powerful method. The SVM algorithm is based on kernel-functions like radial, linear, neural, exponential, sigmoid, polynomial, anova, multiquadric, hybrid, etc. (Ağbulut et al., 2020a). In the present study, a radial basis function was utilized as the kernel function. Accordingly, the optimum iteration number was found to be 1.E9 for each response. Other parameters, kernel gamma, and C to train were taken as 0.18, and 220 for COP, 0.061 and 600 for gained energy, and 0.11 and 800 for efficiency.

To make a comparison between the ANN and SVM algorithms, four metrics are discussed in this research. These metrics are the coefficient of determination (R^2), the root-mean-square error (RMSE), mean bias error (MBE), and mean absolute percentage error (MAPE). Their formulas are given below (Bakay and Ağbulut, 2021):

$$R^2 = 1 - \frac{\sum (y_i - x_i)^2}{\sum (x_i - \overline{x}_i)^2}, \tag{7}$$

$$\text{RMSE} = \sqrt{\frac{1}{n} \sum_{i=1}^{n} (y_i - x_i)^2}, \tag{8}$$

$$\text{MBE} = \frac{1}{n} \sum_{i=1}^{n} (y_i - x_i), \tag{9}$$

$$\text{MAPE} = \frac{1}{n} \sum_{i=1}^{n} \left| \frac{x_i - y_i}{x_i} \right| \times 100. \tag{10}$$

In the relevant equations, n is the number of observations, y_i and x_i demonstrate the predicted and measured data, respectively, and $\overline{x}_i$ illustrates the arithmetically averaged data experimentally measured in the study.

3. THEORETICAL ANALYSIS

3.1 Energy Analysis

Mass conversation in the air heating system can be expressed by the following equation:

$$\sum \dot{m}_{in} = \sum \dot{m}_{ou} . \tag{11}$$

The Reynolds number can be used to analyze the flow behavior of the air inside the system and can be calculated as follows (Khanlari et al., 2020):

$$\mathrm{Re} = \frac{\rho V D_{\mathrm{hyd}}}{\mu} , \tag{12}$$

where ρ denotes the density, V represents the velocity, D_{hyd} is the hydraulic diameter, and μ represents the dynamic viscosity.

The convective heat transfer coefficient for fluid (air) flowing over the absorber surface can be expressed as

$$h = \frac{k}{D_{\mathrm{hyd}}} \mathrm{Nu} . \tag{13}$$

Here, k indicates the thermal conductivity and Nu represents the Nusselt number which can be found from the following equation:

$$\mathrm{Nu} = \frac{h D_{\mathrm{hyd}}}{k} . \tag{14}$$

The specific heat of flowing air can be expressed as follows (Zare et al., 2006):

$$c_p = 1009.26 - 0.0040403 T_a + 0.00061759 {T_a}^2 - 0.0000004097 {T_a}^3 . \tag{15}$$

The mass flow rate of air could be found by utilizing the following expression:

$$\dot{m}_a = \rho_a \dot{V}_a , \tag{16}$$

where $\dot{V}_a$ demonstrates the volume flow rate of air and ρ_a represents the density of air and can be calculated as follows (Tiwari, 2002):

$$\rho_a = 353.44/T_a . \tag{17}$$

The heat energy gained by the TSHs can be calculated as (Abuşka and Şevik, 2017)

$$\dot{Q}_u = A_{as} F_R \left[(\tau\alpha) I - U_{\mathrm{loss}} A_{as} \left(T_{as} - T_{aa} \right) \right] . \tag{18}$$

Here, F_R represents the heat removal factor that can be found from the following equation:

$$F_R = \frac{\dot{m}_a c_p \left(T_{as} - T_{aa} \right)}{A_{as} \left[(\tau\alpha) I - U_{\mathrm{loss}} \left(T_{as} - T_{aa} \right) \right]} . \tag{19}$$

Heat losses include convection ($\dot{Q}_{\mathrm{conv}}$), conduction ($\dot{Q}_{\mathrm{cond}}$), and radiation losses ($\dot{Q}_{\mathrm{rad}}$) and can be expressed as

$$\dot{Q}_{\text{loss}} = \dot{Q}_{\text{cond}} + \dot{Q}_{\text{conv}} + \dot{Q}_{\text{rad}} = U_{\text{loss}} A_{as} \left(T_{as} - T_{aa}\right). \tag{20}$$

The energy reflected from the absorber surface can be found as follows:

$$\dot{Q}_{\rho} = \rho\tau I A_{as}. \tag{21}$$

The thermal efficiency of the TSHs could be calculated by (Güler et al., 2020)

$$\eta_t = \frac{\dot{m}_a c_p \left(T_{ou} - T_{in}\right)}{A_{as} I} = F_R \left(\tau\alpha\right) - F_R U_{\text{loss}} \frac{\left(T_{ou} - T_{in}\right)}{I}. \tag{22}$$

It is better to state that a half of heater's total area was used in calculations considering similar studies where tubular-type SHs are investigated (Afshari et al., 2020; Sözen et al., 2020).

The coefficient of performance could be calculated by the following equation (Abuşka and Şevik, 2017; Tuncer et al., 2020):

$$\text{COP} = \frac{\dot{m}_a c_p \left(T_{ou} - T_{in}\right)}{\dot{W}_f}, \tag{23}$$

where $\dot{W}_f$ is the fan power.

In the experimental analysis, solar radiation, voltage–current, temperature, and velocity have been obtained by using proper measurement. Uncertainty analysis is a useful method to attain uncertainties and to evaluate the experimental outcomes. The uncertainties could arise from device accuracy, calibration of the utilized device, reading, experimental conditions, and connection type (Sözen et al., 2019; Çiftçi and Sözen, 2021). A general expression for experimental uncertainty can be given as follows (Ağbulut et al., 2020b; Karagöz et al., 2020):

$$W_R = \left[\left(\frac{\partial R}{\partial x_1} w_1\right)^2 + \left(\frac{\partial R}{\partial x_2} w_2\right)^2 + \ldots + \left(\frac{\partial R}{\partial x_n} w_n\right)^2\right]^{1/2}. \tag{24}$$

Here, w_1, w_2, and w_n are the uncertainties in the independent variables and W_R is the total uncertainty.

The uncertainty for working fluid (air) mass flow rate can be calculated by the following equation:

$$W_R = \left[\left(\frac{\partial \dot{m}}{\partial V} wV\right)^2 + \left(\frac{\partial \dot{m}}{\partial D} wD\right)^2 + \left(\frac{\partial \dot{m}}{\partial \rho_a} w\rho_a\right)^2\right]^{1/2}. \tag{25}$$

Uncertainties for absorber surface area and thermal efficiency can be found by Eqs. (26) and (27), respectively:

$$W_{A_{as}} = \left[\left(\frac{\partial A_{as}}{\partial L} wL\right)^2 + \left(\frac{\partial A_{as}}{\partial W} wW\right)^2 + \left(\frac{\partial A_{as}}{\partial r} wr\right)^2\right]^{1/2}, \tag{26}$$

$$W_{\eta_t} = \left[\left(\frac{\partial \eta_t}{\partial \dot{m}} w\dot{m}\right)^2 + \left(\frac{\partial \eta_t}{\partial c_p} wc_p\right)^2 + \left(\frac{\partial \eta_t}{\partial \Delta T} w\Delta T\right)^2 + \left(\frac{\partial \eta_t}{\partial A_{as}} wA_{as}\right)^2 + \left(\frac{\partial \eta_t}{\partial I} wI\right)^2\right]^{1/2}. \tag{27}$$

3.2 Enviro-Economic Evaluation

The capital cost can be found by considering the cost of used materials and labor cost. In a basic solar heater, used materials consist of absorber plate, transparent cover, piping, and thermal insulation materials. In a study

performed by Ural (2019), the costs of solar heaters were reported in the range of 224–337 USD. Instead of conventional materials, waste materials have been used for air heating applications in this study. In capital cost calculations, a low power consuming axial fan (40 W), a dimmer switch, paint, sealants, and fittings have been considered for tubular-type solar heaters. The total investment cost for each heater is 21 USD. The salvage value SV can be found as follows:

$$\mathrm{SV} = C_{\mathrm{cost}}/5\,. \tag{28}$$

The cost of solar heater after n years can be calculated by the following equation (Deniz and Çınar, 2016):

$$C_{\mathrm{solarheater}} = C_{\mathrm{cost}}\left(1+i\right)^{n}. \tag{29}$$

The capital recovery factor can be obtained as follows:

$$C_{\mathrm{recoveryfactor}} = \left[i\left(1+i\right)^{n}\right]\Big/\left[\left(1+i\right)^{n}-1\right]. \tag{30}$$

The cost of unit obtained energy could be defined as

$$C_{u} = AC/365(E_{\mathrm{useful}})\,. \tag{31}$$

Levelized cost of heating is an important indicator to evaluate solar heaters economically. This parameter shows the feasibility of the heating system and can be found by the following equation (Abuşka and Şevik, 2017):

$$\mathrm{LCOH} = \frac{C_{\mathrm{cost}}C_{\mathrm{recoveryfactor}} + \mathrm{AMC}}{E_{\mathrm{collector}}}. \tag{32}$$

The simple payback period is expressed as the time it takes to cumulative savings that is equal to the total initial investment. In other words, the simple payback period is the time needed to recover the cost of the system and used to assess the feasibility of the investment. The average lifespan of the solar heater is about 20 years (Ural, 2019; Abuşka and Şevik, 2017). So, the simple payback period should be less than 20 years. The simple payback period is calculated as follows:

$$\mathrm{SPBP} = \frac{C_{\mathrm{cost}}}{\mathrm{FCS} + \phi_{\mathrm{CO_2}}}. \tag{33}$$

The fuel consumption saving (FCS) is

$$\mathrm{FCS} = E_{h}/\eta_{t}\,, \tag{34}$$

where E_h is the annual energy generated by the TSH.

The enviro-economic cost Z_{CO2} is the annual income of CO_2 reduction and it is found as

$$Z_{\mathrm{CO_2}} = \mathrm{CP}_{\mathrm{CO_2}}\phi_{\mathrm{CO_2}}\,. \tag{35}$$

Here, $\mathrm{CP_{CO2}}$ is the average international carbon price taken as 14.5 \$/tCO_2 (Abuşka and Şevik, 2017). The annual CO_2 saved on the basis of overall thermal energy is estimated by the following equation (Tripathi et al., 2016):

$$\phi_{\mathrm{CO_2}} = \frac{\mathrm{CDA}\left(Q_{u}\right)}{1000}. \tag{36}$$

Emissions of CO_2 from fuel combustion can be found as

$$\mathrm{EM}_{\mathrm{CO_2}} = \mathrm{EC}_{f}\left(\psi_{\mathrm{CO_2}}\right), \tag{37}$$

where ψ_{CO2} is the average CO_2 equivalent intensity for electricity generation (0.523 kg CO_2/kWh) (Abuşka and Şevik, 2017) and EC_f presents the yearly energy consumption of fan.

4. RESULTS AND DISCUSSION

4.1 Numerical Results

In this section, numerical simulation findings are illustrated and explained. The main aim of the numerical simulation of tubular-type TSHs is to demonstrate the applicability of this type of solar heaters. Figure 6 shows the temperature contour in TSHs designed by using sheet metal material with two different diameters and at three mass flow rates. It is clearly seen in Fig. 6 that increasing flow rate leads to decrease in the outlet temperature in

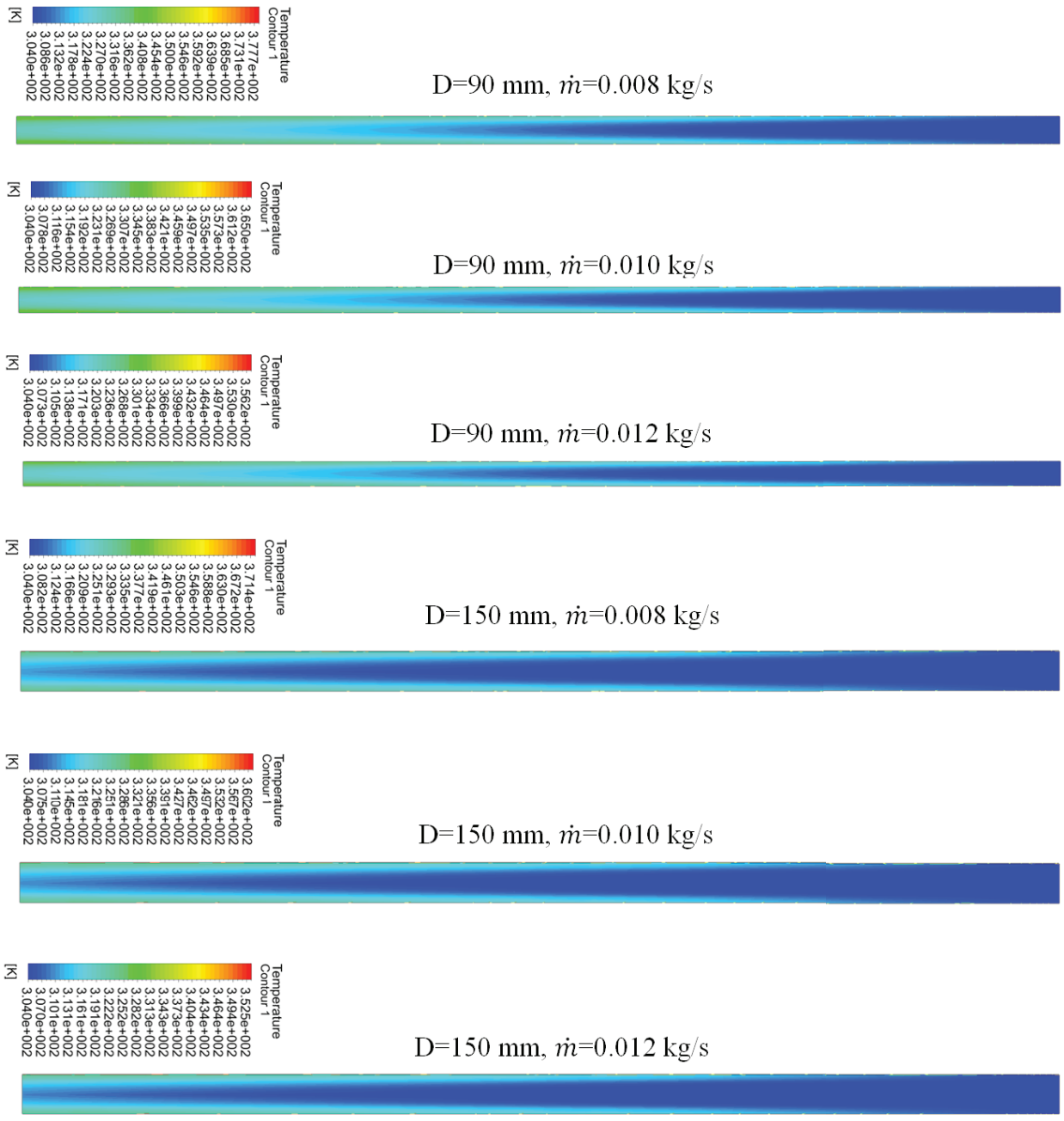

FIG. 6: Temperature contour in TSHs with two different diameters and at three mass flow rates

both TSHs with different diameters. In addition, increasing the diameter of TSH causes a reduction in the thermal energy gain at all flow rates. By increasing the diameter of the tube, the air in the middle region of the tube cannot absorb heat energy and consequently cannot warm up. In other words, increasing the tube diameter leads to compression of a dead zone in the middle region of the tube.

Figure 7 presents the outlet temperature of TSHs with sheet metal material depending on the diameter and flow rate. As is expected, increasing flow rate led to a reduction in the outlet temperature of TSHs. Also, increasing the diameter of the tube caused a decrease in the outlet temperature. Decreasing the diameter from 150 mm to 90 mm led to an improvement in the outlet temperature by 18%, 21.5%, and 24% at 0.012, 0.010, and 0.008 kg/s mass flow rates, respectively. The numerical results indicated that a tubular-type heater with 90-mm diameter showed better thermal performance than TSH with 150-mm diameter. Consequently, in the experimental setup, the tube with 90-mm diameter has been utilized.

4.2 Experimental Results

Performance tests of tubular solar heaters have been conducted under clear sky conditions. The tests have been carried out at two tilt angles including 90^o (Exps. 1–3) and 32^o (experiments 4–6). Figure 8 presents hourly measured solar radiation values during the performance tests. The mean daily solar radiation value in experiments 1, 2, 3, 4, 5, and 6 was measured as 714, 763, 734, 932, 981, and 958 W/m^2, respectively. As can be seen in Fig. 8, solar radiation starts to increase in the morning and reaches a maximum value at noon and then starts to reduce in the afternoon. Also, the effect of tilt angle on solar radiation values is obviously seen in Fig. 8. The maximum solar radiation value achieved was 1127 W/m^2 in experiment 5.

The hourly variation of ambient temperature during the experiments is illustrated in Fig. 9. The ambient temperature exhibited a similar trend with solar radiation and reached a maximum value at noon as expected.

Figure 10 demonstrates the variation of gained energy with time in MTSH and PTSH at different flow rates. Average gained energy values at 0.008, 0.010, and 0.012 kg/s and 32^o tilt angle are 208.11, 228.60 and 233.78 W, respectively. Also, average gained energy values in PTSH at 0.008, 0.010 and 0.012 kg/s and 32^o tilt angle are 190.42, 213.45 and 216.01 W, respectively. Average gained energy values in MTSH at 0.008, 0.010, and 0.012 kg/s and 90^o tilt angle are 151.19, 159.81, and 162.30 W, respectively. Also, average gained energy values in PTSH at 0.008, 0.010, and 0.012 kg/s and 90^o tilt angle are 131.53, 136.48, and 141.70 W, respectively. Moreover, the maximum gained energy value obtained was 327.10 W at 0.012 kg/s at angular placement using MTSH at 13:00. Raising the air flow rate in the SHs leads to improvement in the gained energy. Consequently, thermal

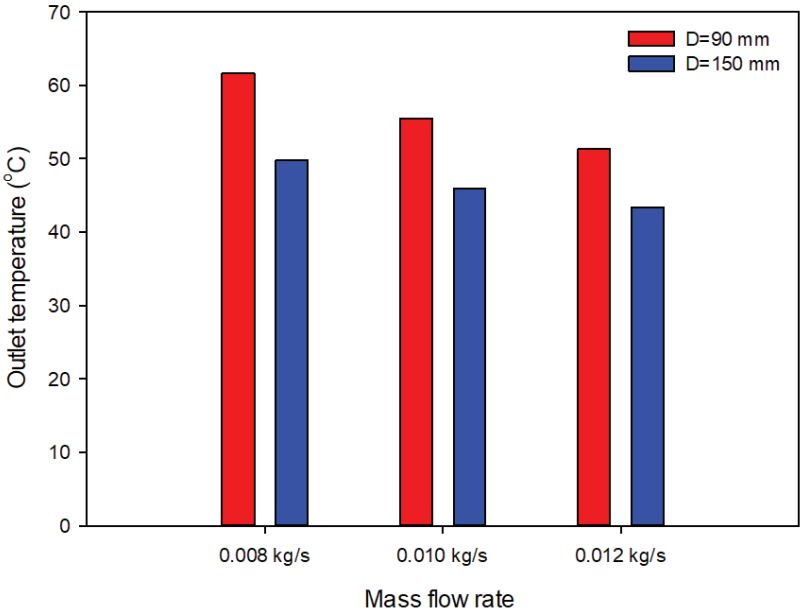

FIG. 7: Outlet temperature of TSHs depending on diameter and flow rate

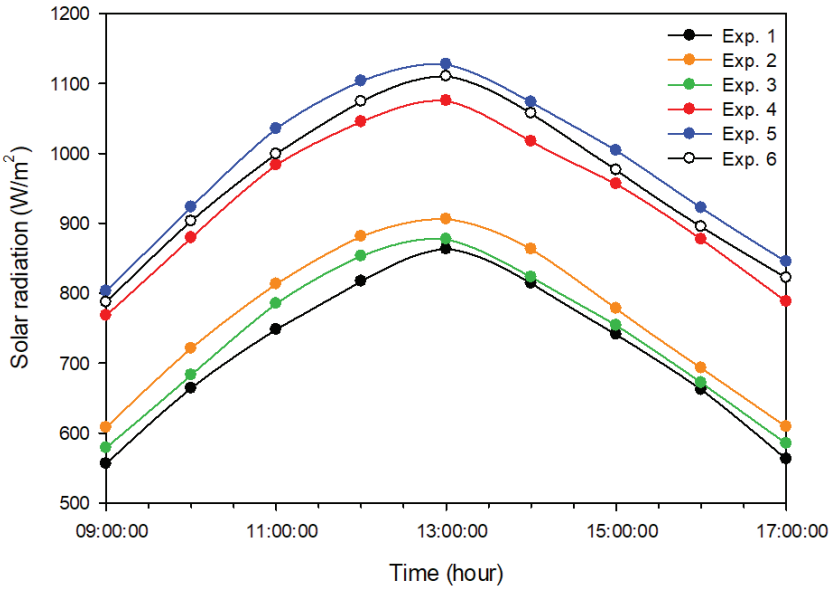

FIG. 8: Solar radiation variation during the tests

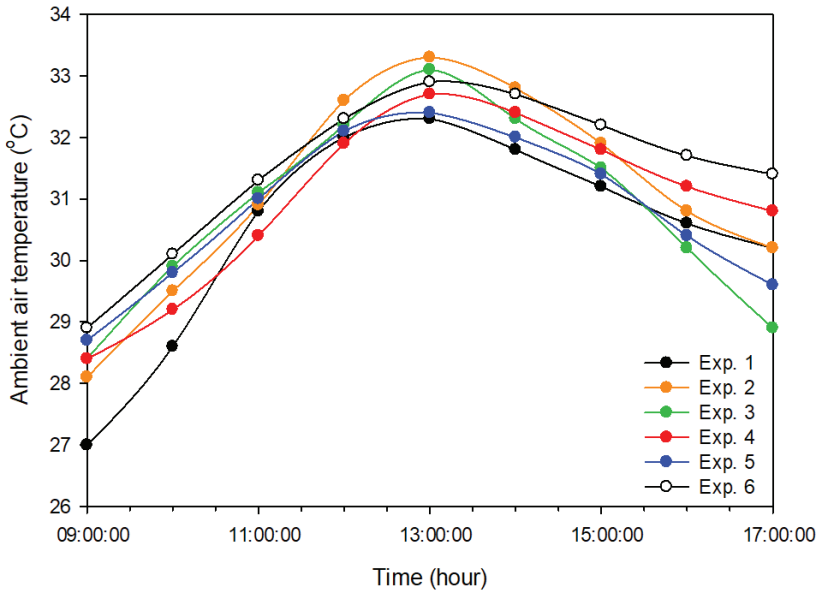

FIG. 9: Hourly variation of ambient air temperature

efficiency is increased by improving the gained energy in the solar air heater. Therefore, the air flow rate is a significant parameter in SHs which should be taken into consideration (Güler et al., 2020; Ceylan et al., 2013). Also, it should be indicated that optimizing the air flow depends on the desired outlet temperature.

Figure 11 demonstrates hourly variation of thermal efficiency in MTSH and PTSH at different flow rates. Average thermal efficiency values in MTSH at 0.008, 0.010, and 0.012 kg/s and 32^o tilt angle are 38.46%, 44.01%, and 50.96%, respectively. Also, average thermal efficiency values in PTSH at 0.008, 0.010, and 0.012 kg/s and 32^o tilt angle are 35.10%, 41.01%, and 47.06%, respectively. Average thermal efficiency values in MTSH at 0.008, 0.010, and 0.012 kg/s and 90^o tilt angle are 36.33%, 39.30%, and 45.74%, respectively. Also, average thermal efficiency

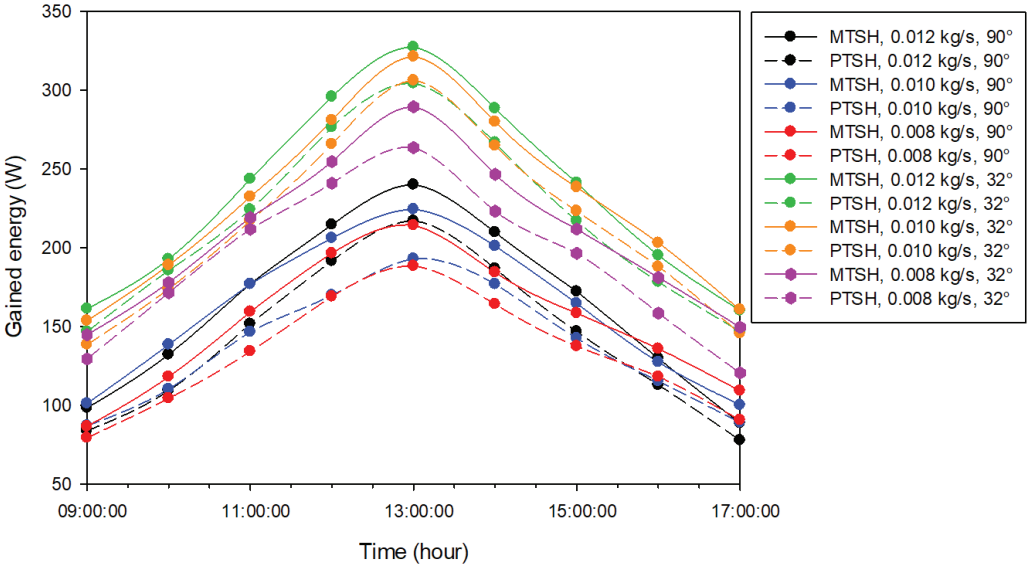

FIG. 10: Variation of gained energy with time

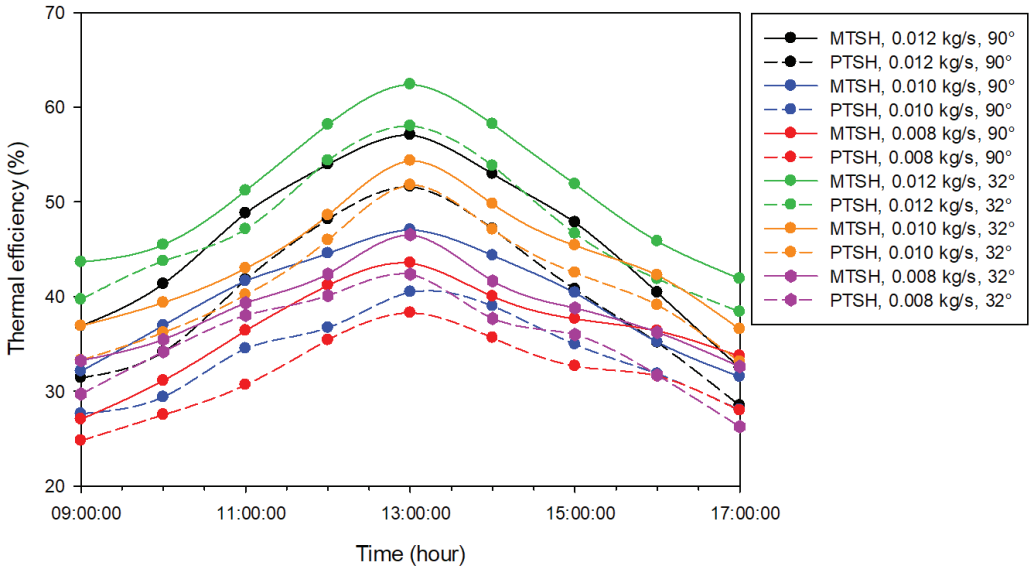

FIG. 11: Hourly variation of thermal efficiency

values in PTSH at 0.008, 0.010, and 0.012 kg/s and 90^{o} tilt angle are 31.60%, 33.61%, and 39.84%, respectively. Moreover, the highest thermal efficiency value obtained was 62.41% at 0.012 kg/s at angular placement using MTSH at 13:00. In a study done by Kishk et al. (2019), aluminum cans were integrated to a single-pass solar heater to be used in the drying of agricultural products. They obtained thermal efficiency between 22–65% (Kishk et al., 2019). In another study performed by Al-Damook et al. (2019), aluminum cans were integrated to a double-pass SH and the maximum thermal efficiency obtained was 60.2% (Al-Damook et al., 2019). In another study, aluminum cans were utilized to enhance the performance of double-pass SH and the maximum thermal efficiency achieved was 70% (Ozgen et al., 2009). By comparing the obtained thermal efficiency in this work with similar studies in the literature, we can say that reused waste sheet metal and plastic materials can be effectively utilized in

solar thermal applications. Şevik and Abuşka (2020) utilized tubular foil ducts as absorber in a single-flow SH to improve the thermal efficiency. They stated that using tubular foil ducts as absorber increased the thermal efficiency by 18.82% in comparison to the flat plate absorber. Abo-Elfadl et al. (2021) used aluminum tubes to develop a tubular SH with casing and compared it with another SH with flat absorber. They indicated that using tubular absorber improved the performance of SH notably and obtained the highest thermal efficiency for tubular SH as 86%. Using aluminum tubes with high thermal conductivity and casing is the main factor that resulted in obtaining high thermal efficiency. Yassien et al. (2020) added tubes on absorber surfaces of a triple-pass SH and achieved the thermal efficiency approximately between 31–80%. Murali et al. (2020b) used tubular absorber to develop a tubular SH and added fins to increase the overall performance. They attained maximum efficiency of SH as 65%. The obtained thermal efficiencies of tubular-type heaters utilized in this research are in good agreement with related works. In addition, in this work, the solar air heaters were manufactured from reused waste materials, while in other studies recycled or reused materials were not directly utilized in manufacturing solar heaters and, generally, they have been used as auxiliary materials to enhance the performance of SHs.

COP is another indicator used by many researchers in evaluating SHs. Figure 12 presents the hourly variation of COP values in MTSH and PTSH at different flow rates. Mean COP values in MTSH at 0.008, 0.010, and 0.012 kg/s flow rates and 32^{o} tilt angle are 5.50, 6.29, and 6.75, respectively. Also, mean COP values in PTSH at 0.008, 0.010, and 0.012 kg/s and 32^{o} tilt angle are 4.78, 5.72, and 6.23, respectively. Mean COP values in MTSH at 0.008, 0.010, and 0.012 kg/s and 90^{o} tilt angle are 3.80, 4.28, and 4.69, respectively. Also, mean COP values in PTSH at 0.008, 0.010, and 0.012 kg/s and 90^{o} tilt angle are 3.31, 3.66, and 4.09, respectively. Moreover, the maximum COP value obtained was 9.39 at 0.012 kg/s at angular placement using MTSH. In an experimental research performed by Khanlari et al. (2020), COP value was attained in the range of 3.4–4 for a tubular-type solar heater. In another research conducted by Güler et al. (2020), metallic mesh modification integration was utilized to upgrade the performance of a solar heater. They obtained COP values in the range of 4.83–5.53. The obtained COP values in this study are higher in comparison with available studies in the literature. However, it should be indicated that high temperature difference values were obtained in this study with lower fan power consumption. This result clearly demonstrates the successful application of this simple tubular-type solar heater manufactured from waste materials.

Figure 13 illustrates the numerically and experimentally obtained temperature difference in MTSH and PTSH with respect to mass flow rate. In this study, different viscous models have been examined to determine the most suitable model. As can be clearly seen in Fig. 13, the RNG k–ε model gave the most accurate results when compared to the experimental findings. Both experimental and CFD simulation results indicated higher temperature differences obtained by MTSH in comparison with PTSH. Metal material has a higher thermal conductivity in

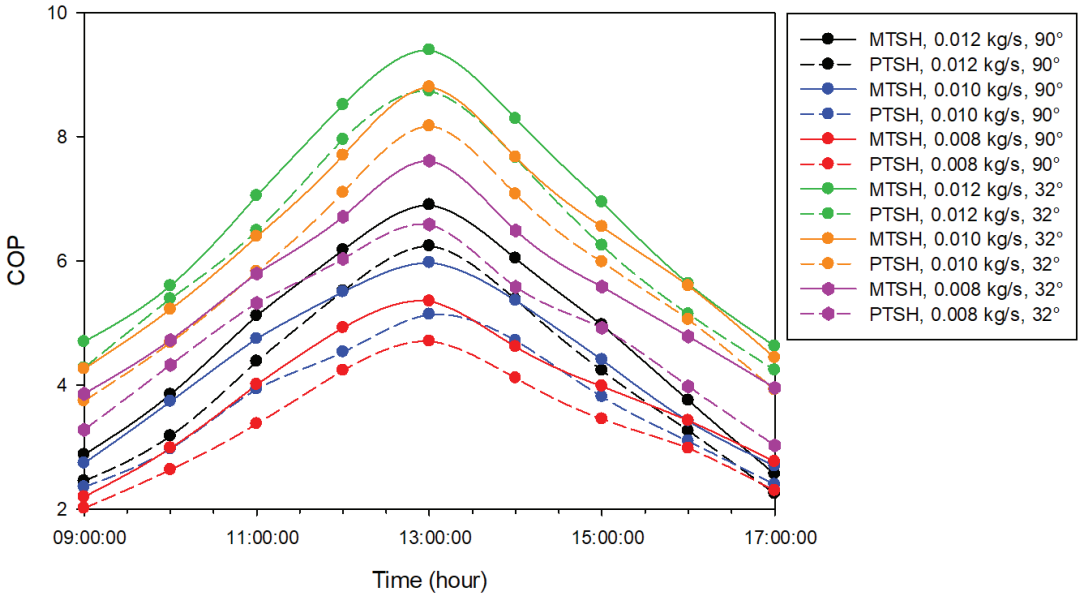

FIG. 12: Hourly variation of COP

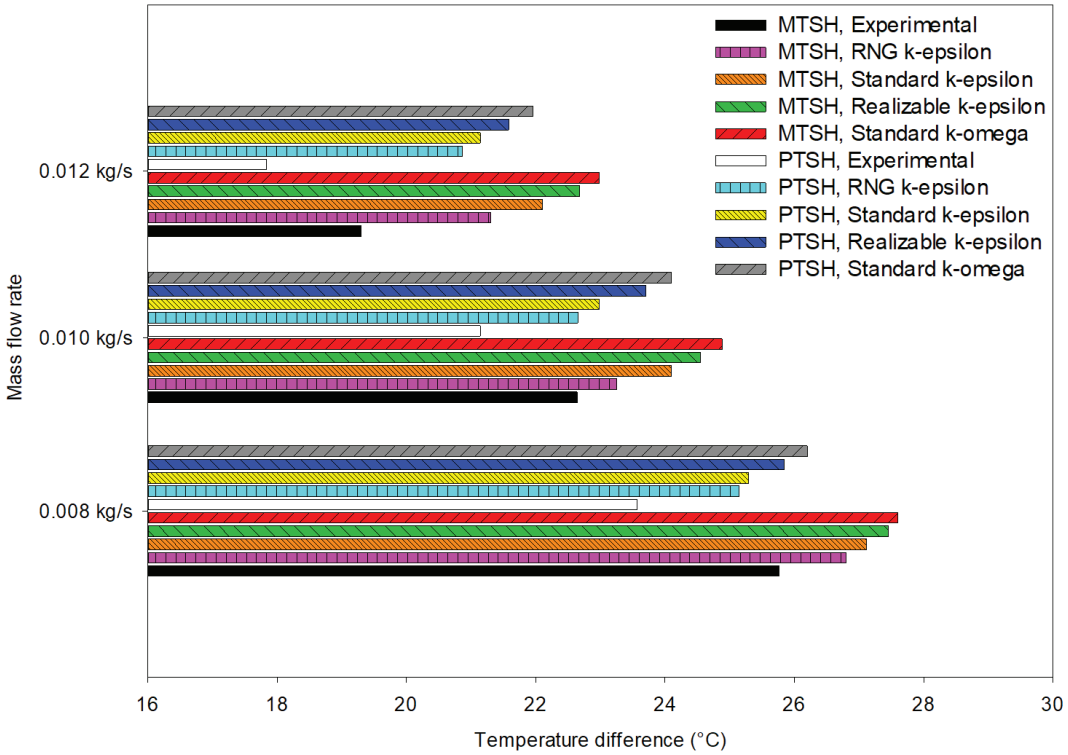

FIG. 13: Numerical and experimental temperature difference in TSH

comparison to plastic material. Therefore, in the tubular heater with sheet metal, the energy absorbed by a tube is transferred to the flowing air at higher rates in comparison to the tubular heater with plastic material. It is better to highlight that the tubular heater with sheet metal exhibited better performance than the other one. However, the thermal performance of the tubular heater with plastic material is in an acceptable range which shows its applicability. The numerically obtained temperature differences in MTSH and PTSH are in the range of 21.3–26.8 and 20.86–25.14^{o}C, respectively. In addition, the experimentally obtained temperature differences in MTSH and PTSH are in the range of 19.3–25.76 and 17.83–23.57^{o}C, respectively.

Table 2 presents the uncertainty of some parameters in the experiments. The obtained uncertainty values are within an acceptable range when compared to similar studies in the literature (Naghdbishi et al., 2020; Ceylan and Gürel, 2016; Tuncer et al., 2020; Khanlari et al., 2020).

TABLE 2: The uncertainty of some parameters

Parameter	Unit	Uncertainty
Air velocity	m/s	± 0.29
Temperature	^{o}C	± 0.55
Electrical power	W	± 0.32
Solar radiation	W/m^2	± 17.22
Thermal efficiency	%	± 0.92
COP	%	± 3.78

Simple payback period values for plastic and metal solar heaters for wall-mounted placement were found in the range of 1.59–1.71 years and 1.39–1.49 years, respectively. Payback values for angular placement were obtained to be in the range of 1.04–1.08 and 0.96–1.08 years, respectively. In their study, Abuşka and Şevik (2017) found these values in the range of 4.3–4.6 years. Also, Banout et al. (2011) obtained payback period as 3.26 years for a double-flow solar heater. According to the results, the payback period can be reduced by less than 1 year with the use of waste materials in the manufacturing process of solar air heaters.

In this study, LCOH values were obtained for plastic- and metal-based heaters in the range of 0.39–0.64 $-ct/kWh and 0.36–0.56 $-ct/kWh, respectively. Lillo et al. (2017) found LCOH values in the range of 2.5–17 $-ct/kWh/m^2 for concentrated solar heating systems. In the study done by Mauthner and Weiss (2016), LCOH values were obtained between 1.6 and 5 €-ct/kWh. It should be stated that the mentioned studies have higher capital costs. With the use of metal and plastic wastes, the capital cost of SHs can be minimized.

Enviro-economic costs for metal and plastic solar heaters were obtained as 8.02 and 7.55 $/year. Abuşka and Şevik (2017) found these values between 4.5 and 5.8 $/year. Tiwari et al. (2015) obtained this parameter as 6.29 $/year for a photovoltaic solar heater for a desalination system. In the study performed by Bait (2019), which investigates a solar heater-based solar still, an enviro-economic cost of 4.42 $/year was achieved. As can be seen, the findings of the present study are in good agreement with similar studies of solar energy-based heating systems.

A comparison of different solar air heating applications is given in Table 3. Some of the available studies presented in Table 3 developed solar air heaters by reusing waste materials like aluminum cans and exhibited the potential of using waste materials in solar heating systems. In addition, in some researches various tubular SHs have been given to make a comparison between them and the obtained results of tubular SHs tested in this study. In Table 3 test conditions like solar radiation, mass flow rate, and obtained thermal efficiency are given to make a good comparison between the given studies and the present work. As is seen, various absorber plate materials have been used in the given studies. As is known, absorber material has an important effect on the thermal performance of the solar heating system. However, the cost of the utilized absorber plate is another important factor that should be taken into account. Also, some researchers utilized different waste materials which have lower thermal conductivity values in comparison to conventional absorber materials with high thermal conductivities. Nevertheless, the solar heating systems with these absorber materials have compatible thermal efficiency in comparison with solar heaters with overpriced absorber materials. In the present work, galvanized sheet and plastic have been used as absorber plate material in solar heating systems. It is better to indicate that materials utilized in this study do not have high thermal conductivity in comparison with ordinary absorber materials like copper and aluminum. However, developed TSHs have acceptable thermal performance in comparison with more complex SHs in the literature. Moreover, the cost of the developed heaters in this work is low in comparison with some related studies that gave the total cost of the system. In general, the results obtained in this work indicated the potential of reusing waste materials in manufacturing solar air heating systems.

4.3 ANN and SVM Modeling Results

Table 4 presents a comparison between the ANN and SVM algorithms relative to R^2, RMSE, MBE, and MAPE.

As can be seen from Table 4, R^2 values for all responses are varying from 0.9293 and 0.9903 for ANN and SVM algorithms. As is well known, R^2 value changes from 0 to 1 and it is desired that it gets close to 1. In general, R^2 values for both ANN and SVM algorithms are calculated to be very close to each other as can be seen in Table 4. However, the R^2 value of the SVM algorithm is seen to be higher than that of the ANN algorithm in all responses. This means that the curves of the data predicted by SVM are very close to those of measured data as compared to the curves of the ANN algorithm. The highest R^2 value is found in COP for both ANN and SVM and its values are 0.9798 and 0.9903 for ANN and SVM, respectively. On the other hand, the lowest R^2 value is also seen in the prediction of efficiency data for both ANN and SVM as seen in Table 4. Another metric to be discussed in the study is RMSE. It is always positive and it is desired that RMSE is close to zero. With this viewpoint, the best results for the RMSE metric were observed in the COP response for both ANN and SVM algorithms. RMSE results of this response are equal to 0.336 and 0.192 for ANN and SVM, respectively. After that, efficiency response has a relatively low RMSE result for both algorithms. On the other hand, the worst RMSE results are noticed to be 10.015 W and 8.546 W for ANN and SVM, respectively. As follows from the comparison of two algorithms, always SVM has better RMSE results than those of the ANN algorithm

TABLE 3: Comparison between different solar air heating applications

Ref.	Application		Application Type	Absorber Material	Mass Flow Rate, kg/s	Solar Radiation, W/m^2	Useful Heat Gain, W	Thermal Efficiency, %	Cost
	Exp.	Num.							
Wang et al. (2020)	✓	X	Multiple S-shaped ribs with gaps	Wood	0.0025, 0.005, 0.007, 0.0097 0.0138, 0.0195	450–650	128.44–459.03	13–48	—
Ozgen et al. (2009)	✓	X	Double-pass solar air heater	Aluminum cans	0.03, 0.05	1003–905	—	20–75	—
Singh et al. (2020)	✓	✓	Double-pass solar air heater	Softwood	0.01–0.05	900	—	74 (average)	—
Abo-Elfadl et al. (2020)	✓	X	Double-pass solar air heater	Aluminum	0.025, 0.05, 0.075	750	—	77.5 (average)	—
Abo-Elfadl et al. (2021)	✓	X	Single- and double-pass tubular solar air heaters	Aluminum tubes	0.025, 0.05, 0.075	802	—	86 (maximum)	—
Şevik and Abuşka (2020)	✓	X	Single-pass tubular and flat-plate solar air heaters	Aluminum foil ducts	0.013, 0.03	929–967	—	65 (maximum)	—
Abdullah et al. (2018)	✓	X	Double-pass solar air heater with turbulators	Aluminum	0.02–0.05	1100	—	68 (maximum)	—
Hassan and Abo-Elfadl (2018)	✓	X	Double-pass solar air heater with corrugated absorber plate	—	0.09	1100	600–1300	82 (maximum)	—
Hassan et al. (2020)	✓	X	Tubular solar air heater	Aluminum tubes	0.025, 0.05, 0.075	750	—	59.8–83.6 (average)	ϕ
Sözen el al. (2020)	✓	✓	Tubular solar air heaters with and without iron mesh	Sheet metal tubes	0.009, 0.011, 0.014	1074	—	51.19–67.69 (average)	—

TABLE 3: (*continued*)

Ref.	Application		Application Type	Absorber Material	Mass Flow Rate, kg/s	Solar Radiation, W/m^2	Useful Heat Gain, W	Thermal Efficiency, %	Cost
	Exp.	Num.							
Afshari et al. (2020)	✓	✓	Tubular solar air heaters with and without turbulators	Sheet metal tubes	0.009, 0.011, 0.013, 0.015	1169	—	47.73–64.13 (average)	—
Abdullah et al. (2017)	✓	X	Single-pass plastic solar air heater with circular cross section	Plastic	0.05–0.25	1000	—	47 (average)	—
Ho et al. (2012)	✓	X	Double-pass solar air heater with baffles and fins	—	0.077	830–1100	—	60 (average)	—
Hernández and Quiñonez (2013)	✓	X	Double-pass solar air heater	—	0.044	1050	900–1200	62 (average)	—
Kabeel et al. (2018)	✓	X	Single-pass solar air heater with finned plate	—	0.04	1030	—	57 (average)	109 USD
Murali et al. (2020a)	✓	X	Solar air heater	Aluminum cans	0.025, 0.0916	800–1400	—	69.8 (average)	—
Kishk et al. (2019)	✓	X	Solar dryer	Aluminum cans	0.005, 0.015	100–660	—	21–72	60 USD
Poole et al. (2018)	✓	X	Solar air heater	Plastic	0.064, 0.041, 0.029	700	—	20–60	113 USD/ m^2
Juanicó and Di Lalla (2013)	✓	X	Solar water heater	Plastic	—	600	—	58 (average)	70 USD
Al-Damook et al. (2019)	✓	✓	Multipass solar air heater	Aluminum	0.096, 0.088, 0.0819	600–1050	—	46–60	—
This study	✓	✓	Single-pass tubular heater	Galvanized sheet, plastic	0.008, 0.010, 0.012	714–981	131–234	31.60–50.96	21 USD

TABLE 4: Comparison of algorithms with R^2, RMSE, MBE, and MAPE metrics

Metric	COP		Q		Efficiency	
	ANN	SVM	ANN	SVM	ANN	SVM
R^2	0.9798	0.9903	0.9773	0.9826	0.9293	0.9649
RMSE	0.336	0.192	10.015 W	8.546 W	2.184%	1.759%
MBE	–0.213	–0.056	–1.423 W	–1.379 W	0.011%	–0.601%
MAPE	6.793%	4.316%	5.661%	4.552%	4.843%	3.663%

for all-responses. MBE is another statistical metric used in this study to discuss the prediction results. MBE can take negative or positive results, but it is desired to be close to zero for the MBE metric. If MBE takes negative results, then it means the prediction results are smaller than actual results. With this viewpoint, it is evident from Table 4 that both ANN and SVM algorithms generally have predicted lower values than the actual ones. The SVM algorithm gives better results in terms of the MBE metric for COP and gained energy responses in comparison with those of ANN. The last statistical metric used in this study is MAPE. It gives the percentage of the mean of the absolute values of errors to the absolute values of measured data. As can be seen from Table 4, for all responses, SVM is giving the best results in terms of MAPE metric as compared with that of ANN. MAPE results of all responses are highly close to each other and change from 3.663 to 6.793. Efficiency data has the lowest MAPE results with 4.843 for ANN, 3.663 for the SVM algorithm. On the other hand, among all responses, based on Table 4, it is possible to say that both ANN and SVM algorithms are giving very satisfying results; however, SVM has presented the best results for nearly all metrics. Therefore, SVM is coming to fore for the prediction of COP, gained energy, and efficiency data (Figs. 14–16). Additionally, the most successful prediction results are achieved for COP.

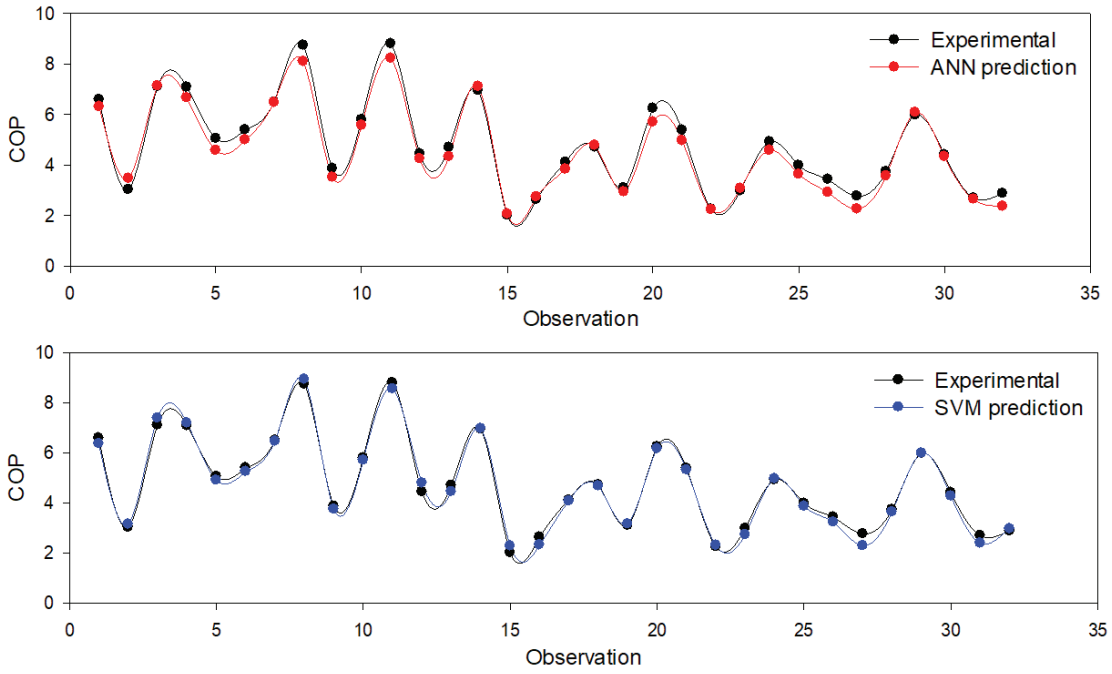

FIG. 14: Prediction results of ANN and SVM algorithms for COP values

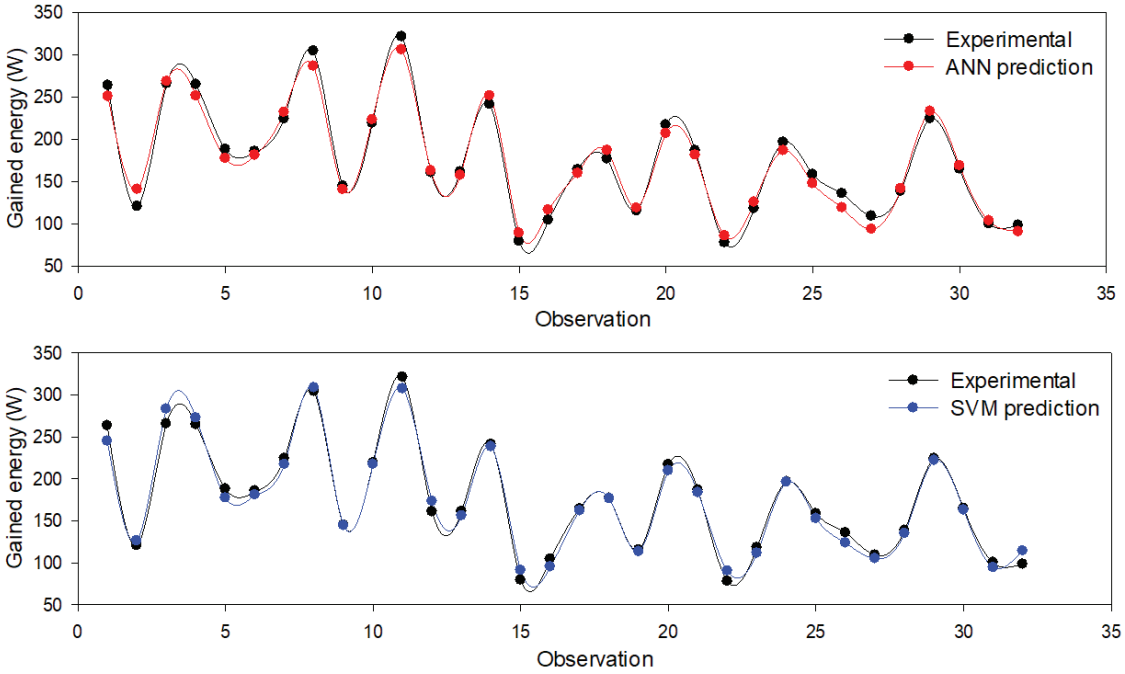

FIG. 15: Prediction results of ANN and SVM algorithms for Q values

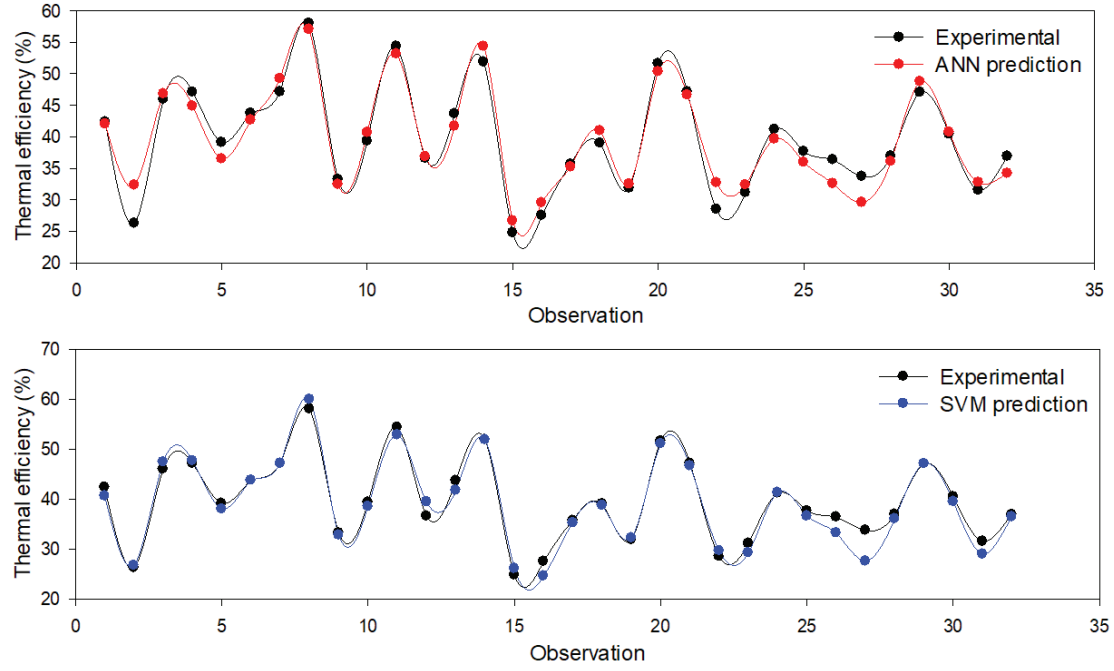

FIG. 16: Prediction results of ANN and SVM algorithms for efficiency values

5. CONCLUSIONS

In the present work, plastic and metal materials are reused in fabricating solar air heaters. Two tubular solar air heaters have been designed, fabricated, and experimented. Firstly, the applicability of tubular-type heaters has been numerically studied. The solar heaters have been tested at two tilt angles including 90^{o} (wall-mounted) and 32° (angular placement) and also at three flow rates including 0.012, 0.010, and 0.008 kg/s. The experimental findings showed that the thermal efficiency of metal tubular heater and plastic tubular heater varied in the range of 36.33–50.96% and 31.60–47.06%, respectively. The obtained COP values in the present work are higher in comparison with available works in the literature when compared to the thermal efficiency. However, it should be indicated that high temperature difference values were obtained in this study with lower fan power consumption which leads to obtaining higher COP values. The outcomes of this study clearly demonstrate the successful application of this simple and cost-effective tubular-type solar heater manufactured from waste materials. Besides this type of tubular heaters, a foldable version of waste material-based solar air heaters can be developed to be utilized in disaster areas and regions with limited access to energy. Moreover, the paper also indicates that the results of COP, gained energy, and efficiency for such a system can be successfully predicted by using ANN and SVM algorithms with very satisfying results. Even if both algorithms give satisfying results, it is possible to say that the SVM algorithm is coming fore in comparison with the ANN algorithm based on the statistical metrics.

REFERENCES

Abdullah, A.S., Abou Al-sood, M.M., Omara, Z.M., Bek, M.A., and Kabeel, A.E., Performance Evaluation of a New Counter-flow Double Pass Solar Air Heater with Turbulators, *Sol. Energy*, vol. **173**, pp. 398–406, 2018.

Abdullah, A.S., El-Samadony, Y.A.F., and Omara, Z.M., Performance Evaluation of Plastic Solar Air Heater with Different Cross-Sectional Configuration, *Appl. Therm. Eng*., vol. **121**, pp. 218–223, 2017.

Abo-Elfadl, S., Hassan, H., and El-Dosoky, M.F., Study of the Performance of Double Pass Solar Air Heater of a New Designed Absorber: An Experimental Work, *Sol. Energy*, vol. **198**, pp. 479–489, 2020.

Abo-Elfadl, S., Yousef, M.S., and Hassan, H., Energy, Exergy, and Enviroeconomic Assessment of Double and Single Pass Solar Air Heaters Having a New Design Absorber, *Process Safety Environ. Protect*., vol. **149**, pp. 451–464, 2021.

Abuşka, M. and Şevik, S., Energy, Exergy, Economic and Environmental (4E) Analyses of Flat-Plate and V-Groove Solar Air Collectors Based on Aluminum and Copper, *Sol. Energy*, vol. **158** pp. 259–277, 2017.

Afshari, F., Sözen, A., Khanlari, A., Tuncer, A.D., and Şirin, C., Effect of Turbulator Modifications on the Thermal Performance of Cost-Effective Alternative Solar Air Heater, *Renew. Energy*, vol. **158**, pp. 297–310, 2020.

Ağbulut, Ü., Gürel, A.E., and Sarıdemir, S., Experimental Investigation and Prediction of Performance and Emission Responses of a CI Engine Fuelled with Different Metal-Oxide Based Nanoparticles–Diesel Blends Using Different Machine Learning Algorithms, *Energy*, vol. **215**, p. 119076, 2021.

Ağbulut, Ü., Gürel, A.E., Ergün, A., and Ceylan, İ., Performance Assessment of a V-Trough Photovoltaic System and Prediction of Power Output with Different Machine Learning Algorithms, *J. Clean. Prod*., vol. **268**, p. 122269, 2020a.

Ağbulut, Ü., Karagöz, M., Sarıdemir, S., and Öztürk, A., Impact of Various Metal-Oxide Based Nanoparticles and Biodiesel Blends on the Combustion, Performance, Emission, Vibration and Noise Characteristics of a CI Engine, *Fuel*, vol. **270**, p. 117521, 2020b.

Aizenshtein, E.M., Bottle Wastes-to-Textile Yarns, *Fibre Chem.*, vol. **47**, pp. 343–347, 2016.

Al-Damook, M., Obaid, Z.A.H., Al Qubeissi, M., Dixon-Hardy, D., Cottom, J., and Heggs, P.J., CFD Modeling and Performance Evaluation of Multipass Solar Air Heaters, *Numer. Heat Transf., Part A: Appl*., vol. **76**, pp. 438–464, 2019.

Bait, O., Exergy, Environ-Economic and Economic Analyses of a Tubular Solar Water Heater Assisted Solar Still, *J. Clean. Prod*., vol. **212**, pp. 630–646, 2019.

Bakay, M.S. and Ağbulut, Ü., Electricity Production Based Forecasting of Greenhouse Gas Emissions in Turkey with Deep Learning, Support Vector Machine and Artificial Neural Network Algorithms, *J. Clean. Prod.*, vol. **285**, p. 125324, 2021.

Banout, J., Ehl, P., Havlik, J., Lojka, B., Polesny, Z., and Verner, V., Design and Performance Evaluation of a Double-Pass Solar Drier for Drying of Red Chilli (*Capsicum annum* L.), *Sol. Energy*, vol. **85**, pp. 506–515, 2011.

Burges, C.J.C., A Tutorial on Support Vector Machines for Pattern Recognition, *Data Mining Knowledge Disc*., vol. **2**, pp. 121–167, 1998.

Ceylan, I. and Gürel, A.E., Solar-Assisted Fluidized Bed Dryer Integrated with a Heat Pump for Mint Leaves, *Appl. Therm. Eng.*, vol. **106**, pp. 899–905, 2016.

Ceylan, İ., Gürel, A.E., and Ergün, A., The Mathematical Modeling of Concentrated Photovoltaic Module Temperature, *Int. J. Hydrog. Energy*, vol. **42**, pp. 19641–19653, 2017.

Ceylan, I., Kaya, M., Gürel, A.E., and Ergün, A., Energy Analysis of a New Design of a Photovoltaic Cell-Assisted Solar Dryer, *Drying Technol.*, vol. **31**, pp. 1077–1082, 2013.

Charvat, P., Klimes, L., Pech, O., and Hejcík, J., Solar Air Collector with the Solar Absorber Plate Containing a PCM—Environmental Chamber Experiments and Computer Simulations, *Renew. Energy*, vol. **143**, pp. 731–740, 2017.

Çiftçi, E. and Sözen, A., Heat Transfer Enhancement in Pool Boiling and Condensation Using H-BN/DCM and SiO_2/DCM Nanofluids: Experimental and Numerical Comparison, *Int. J. Numer. Methods Heat Fluid Flow*, vol. **31**, pp. 26–52, 2021.

Craig, K.J., Slootweg, M., Le Roux, W.G., Wolff, T.M., and Meyer, J.P., Using CFD and Ray Tracing to Estimate the Heat Losses of a Tubular Cavity Dish Receiver for Different Inclination Angles, *Sol. Energy*, vol. **211**, pp. 1137–1158, 2020.

Deniz, E. and Çınar, S., Energy, Exergy, Economic and Environmental (4E) Analysis of a Solar Desalination System with Humidification–Dehumidification, *Energy Convers. Manage*., vol. **126**, pp. 12–19, 2016.

Fidelis, R., Marco-Ferreira, A., Antunes, L.C., and Komatsu, A.K., Socio-Productive Inclusion of Scavengers in Municipal Solid Waste Management in Brazil: Practices, Paradigms and Future Prospects, *Resour., Conserv. Recycl*., vol. **154**, p. 104594, 2020.

Fuldauer, L.I., Ives, M.C., Adshead, D., Thacker, S., and Hall, J.W., Participatory Planning of the Future of Waste Management in Small Island Developing States to Deliver on the Sustainable Development Goals, *J. Clean. Prod.*, vol. **223**, pp. 147–162, 2019.

Galvin, A.P., Ayuso, J., Jimenez, J.R., and Agrela, F., Comparison of Batch Leaching Tests and Influence of pH on the Release of Metals from Construction and Demolition Wastes, *Waste Manage*., vol. **32**, pp. 88–95, 2012.

Gao, M., Wang, D., Liu, Y., Wang, Y., and Zhou, Y., A Study on Thermal Performance of a Novel Glazed Transpired Solar Collector with Perforating Corrugated Plate, *J. Clean. Prod*., vol. **257**, p. 120443, 2020.

Gardas, B.B., Raut, R.D., and Narkhede, B., Identifying Critical Success Factors to Facilitate Reusable Plastic Packaging towards Sustainable Supply Chain Management, *J. Environ. Manage*., vol. **236**, pp. 81–92, 2019.

Güler, H.Ö., Sözen, A., Tuncer, A.D., Afshari, F., Khanlari, A., Şirin, C., and Gungor, A., Experimental and CFD Survey of Indirect Solar Dryer Modified with Low-Cost Iron Mesh, *Sol. Energy*, vol. **197**, pp. 371–384, 2020.

Gunarathne, N., De Alwis, A., and Alahakoon, Y., Challenges Facing Sustainable Urban Mining in the e-Waste Recycling Industry in Sri Lanka, *J. Clean. Prod.*, vol. **251**, p. 119641, 2020.

Gürel, A.E., Ağbulut, Ü., and Biçen, Y., Assessment of Machine Learning, Time Series, Response Surface Methodology and Empirical Models in Prediction of Global Solar Radiation, *J. Clean. Prod*., vol. **277**, p. 122353, 2020.

Gürel, A.E., Exergetic Assessment of a Concentrated Photovoltaic Thermal (CPV/T) System, *Int. J. Exergy*, vol. **21**, pp. 127–135, 2016.

Hadavand, B. and Imaninasab, R., Assessing the Influence of Construction and Demolition Waste Materials on Workability and Mechanical Properties of Concrete Using Statistical Analysis, *Innov. Infrastruct. Solutions*, vol. **4**, p. 29, 2019.

Hassan, H. and Abo-Elfadl, S., Experimental Study on the Performance of Double Pass and Two Inlet Ports Solar Air Heater (SAH) at Different Configurations of the Absorber Plate, *Renew. Energy*, vol. **116**, pp. 728–740, 2018.

Hassan, H., Abo-Elfadl, S., and El-Dosoky, M.F., An Experimental Investigation of the Performance of New Design of Solar Air Heater (Tubular), *Renew. Energy*, vol. **151**, pp. 1055–1066, 2020.

Hernández, A.L. and Quiñonez, J.E., Analytical Models of Thermal Performance of Solar Air Heaters of Double-Parallel Flow and Double-Pass Counter Flow, *Renew. Energy*, vol. **55**, pp. 380–391, 2013.

Ho, C., Chang, H., Wang, R., and Lin, C., Performance Improvement of a Double-Pass Solar Air Heater with Fins and Baffles under Recycling Operation, *Appl. Energy*, vol. **100**, pp. 155–163, 2012.

Hosseini, S.S., Ramiar, A., and Ranjbar, A.A., Numerical Investigation of Natural Convection Solar Air Heater with Different Fins Shape, *Renew. Energy*, vol. **117**, pp. 488–500, 2018.

Juanicó, L.E. and Di Lalla, N., A New Low-Cost Plastic Solar Collector, *ISRN Renew. Energy*, vol. **102947**, pp. 1–10, 2013.

Kabeel, A.E., Hamed, M.H., Omara, Z.M., and Kandeal, A.W., Influence of Fin Height on the Performance of a Glazed and Bladed Entrance Single-Pass Solar Air Heater, *Sol. Energy*, vol. **162**, pp. 410–419, 2018.

Karagöz, M., Ağbulut, Ü., and Sarıdemir, S., Waste to Energy: Production of Waste Tire Pyrolysis Oil and Comprehensive Analysis of Its Usability in Diesel Engines, *Fuel*, vol. **275**, p. 117844, 2020.

Karagoz, S., Afshari, F., Yildirim, O., and Comakli, O., Experimental and Numerical Investigation of the Cylindrical Blade Tube Inserts Effect on the Heat Transfer Enhancement in the Horizontal Pipe Exchangers, *Heat Mass Transf.*, vol. **53**, pp. 2769–2784, 2017.

Kaya, M., Gürel, A.E., Ağbulut, Ü., Ceylan, I., Çelik, S., Ergün, A., and Acar, B., Performance Analysis of Using CuO–Methanol Nanofluid in a Hybrid System with Concentrated Air Collector and Vacuum Tube Heat Pipe, *Energy Convers. Manage.*, vol. **199**, p. 111936, 2019.

Khanlari, A., Sözen, A., Şirin, C., Tuncer, A.D., and Gungor, A., Performance Enhancement of a Greenhouse Dryer: Analysis of a Cost-Effective Alternative Solar Air Heater, *J. Clean. Prod.*, vol. **251**, p. 119672, 2020.

Kırbaş, İ., Tuncer, A.D., Şirin, C., and Usta, H., Modeling and Developing a Smart Interface for Various Drying Methods of Pomelo Fruit (*Citrus maxima*) Peel Using Machine Learning Approaches, *Comput. Elect. Agric.*, vol. **165**, p. 104928, 2019.

Kishk, S.S., ElGamal, R.A., and ElMasry, G.M., Effectiveness of Recyclable Aluminum Cans in Fabricating an Efficient Solar Collector for Drying Agricultural Products, *Renew. Energy*, vol. **133**, pp. 307–316, 2019.

Kong, J., Niu, J., and Lei, C., A CFD Based Approach for Determining the Optimum Inclination Angle of a Roof-Top Solar Chimney for Building Ventilation, *Sol. Energy*, vol. **198**, pp. 555–569, 2020.

Lamnatou, C., Cristofari, C., Chemisana, D., and Canaletti, J.L., Payback Times and Multiple Midpoint/Endpoint Impact Categories about Building-Integrated Solar Thermal (BIST) Collectors, *Sci. Total Environ.*, vol. **658**, pp. 1039–1055, 2019.

Lillo, I., Pérez, E., Moreno, S., and Silva, M., Process Heat Generation Potential from Solar Concentration Technologies in Latin America: The Case of Argentina, *Energies*, vol. **10**, p. 383, 2017.

Mauthner, F. and Weiss, W., Solar Heat Worldwide Markets and Contribution to the Energy Supply 2014, International Energy Agency, 2016.

Minelgaite, A. and Liobikiene G., Waste Problem in European Union and Its Influence on Waste Management Behaviors, *Sci. Total Environ.*, vol. **667**, pp. 86–93, 2019.

Moghimi, P., Rahimzadeh, H., and Ahmadpour, A., Experimental and Numerical Optimal Design of a Household Solar Fruit and Vegetable Dryer, *Sol. Energy*, vol. **214**, pp. 575–587, 2021.

Murali, G., Reddy, K.R.K., Sai Kumar, M.T., Sai Manikanta, J., and Reddy, V.N.K., Performance of Solar Aluminum Can Air Heater Using Sensible Heat Storage, *Mater. Today: Proc.*, vol. **21**, pp. 169–174, 2020a.

Murali, G., Sundari, A.T.M., Raviteja, S., Chanukyachakravarthi, S., and Tejpraneeth, M., Experimental Study of Thermal Performance of Solar Aluminum Cane Air Heater with and Without Fins, *Mater. Today: Proc.*, vol. **21**, pp. 223–230, 2020b.

Naghdbishi, A., Eftekhari Yazdi, M., and Akbari, G., Experimental Investigation of the Effect of Multi-Wall Carbon Nanotube–Water/Glycol Based Nanofluids on a PVT System Integrated with PCM Covered Collector, *Appl. Therm. Eng.*, vol. **178**, p. 115556, 2020.

Nidhul, K., Yadev, A.K., Anish, S., and Arunachala, U.C., Efficient Design of an Artificially Roughened Solar Air Heater with Semicylindrical Side Walls: CFD and Exergy Analysis, *Sol. Energy*, vol. **207**, pp. 289–304, 2020.

Ozgen, F., Esen, M., and Esen, H., Experimental Investigation of Thermal Performance of a Double-Flow Solar Air Heater Having Aluminum Cans, *Renew. Energy*, vol. **34**, pp. 2391–2398, 2009.

Poole, M.R., Shah, S.B., Grimes, J.L., Boyette, M.D., and Stikeleather, L.F., Evaluation of a Novel, Low-Cost Plastic Solar Air Heater for Turkey Brooding, *Energy Sustain. Develop.*, vol. **45**, pp. 1–10, 2018.

Pujara, Y., Pathak, P., Sharma, A., and Govani, J., Review on Indian Municipal Solid Waste Management Practices for Reduction of Environmental Impacts to Achieve Sustainable Development Goals, *J. Environ. Manage.*, vol. **248**, p. 109238, 2019.

Raj, A.K., Kunal, G., Srinivas, M., and Jayaraj, S., Performance Analysis of a Double-Pass Solar Air Heater System with Asymmetric Channel Flow Passages, *J. Therm. Anal. Calorim.*, vol. **136**, pp. 21–38, 2019.

Şevik, S. and Abuşka, M., Enhancing the Thermal Performance of a Solar Air Heater by Using Single-Pass Semi-Flexible Foil Ducts, *Appl. Therm. Eng.*, vol. **179**, p. 115746, 2020.

Shaikh, S., Thomas, K., and Zuhair, S., An Exploratory Study of e-Waste Creation and Disposal: Upstream Considerations, *Resour. Conserv. Recycl.*, vol. **155**, p. 104662, 2020.

Shen, L., Worrell, E., and Patel, M.K., Open-Loop Recycling: A LCA Case Study of PET Bottle-to-Fibre Recycling, *Resour. Conserv. Recycl.*, vol. **55**, pp. 34–52, 2010.

Singh, A., Solid Waste Management through the Applications of Mathematical Models, *Resour. Conserv. Recycl*., vol. **151**, p. 104503, 2019.

Singh, S., Chaurasiya, S.K., Negi, B.S., Chander, S., Nemś, M., and Negi, S., Utilizing Circular Jet Impingement to Enhance Thermal Performance of Solar Air Heater, *Renew. Energy*, vol. **154**, pp. 1327–1345, 2020.

Sözen, A., Khanları, A., and Çiftçi, E., Experimental and Numerical Investigation of Nanofluid Usage in a Plate Heat Exchanger for Performance Improvement, *Int. J. Renew. Energy Develop*., vol. **8**, pp. 27–32, 2019.

Sözen, A., Sirin, C., Khanlari, A., Tuncer, A.D., and Gürbüz, E.Y., Thermal Performance Enhancement of Tube-Type Alternative Indirect Solar Dryer with Iron Mesh Modification, *Sol. Energy*, vol. **207**, pp. 1269–1281, 2020.

Stolarski, M.J., Warmiński, K., Krzyżaniak, M., Olba-Zięty, E., and Stachowicz, P., Energy Consumption and Heating Costs for a Detached House over a 12-Year Period—Renewable Fuels versus Fossil Fuels, *Energy*, vol. **204**, p. 117952, 2020.

Taniguchi, I., Yoshida, S., Hiraga, K., Miyamoto, K., Kimura, Y., and Oda, K., Biodegradation of PET: Current Status and Application Aspects, *ACS Catal.*, vol. **9**, pp. 4089–4105, 2019.

Tansel, B., From Electronic Consumer Products to e-Wastes: Global Outlook, Waste Quantities, Recycling Challenges, *Environ. Int*., vol. **98**, pp. 35–45, 2017.

Tiwari, G.N., *Solar Energy: Fundamentals, Design Modeling and Applications*, New York and New Dehli: CRC Press and Narosa Publishing House, 2002.

Tiwari, G.N., Yadav, J.K., Singh, D.B., Al-Helal, I.M., and Abdel-Ghany, A.M., Exergoeconomic and Enviroeconomic Analyses of Partially Covered Photovoltaic Flat Plate Collector Active Solar Distillation System, *Desalination*, vol. **367**, pp. 186–196, 2015.

Tripathi, R., Tiwari, G.N., and Dwivedi, V.K., Overall Energy, Exergy and Carbon Credit Analysis of N Partially Covered Photovoltaic Thermal (PVT) Concentrating Collector Connected in Series, *Sol. Energy*, vol. **136**, pp. 260–267, 2016.

Tuncer, A.D., Khanlari, A., Sözen, A., Gürbüz, E.Y., Şirin, C., and Gungor, A., Energy–Exergy and Enviro-Economic Survey of Solar Air Heaters with Various Air Channel Modifications, *Renew. Energy*, vol. **160**, pp. 67–85, 2020.

Ural, T., Experimental Performance Assessment of a New Flat-Plate Solar Air Collector Having Textile Fabric as Absorber Using Energy and Exergy Analyses, *Energy*, vol. **188**, p. 116116, 2019.

Wang, D., Liu, J., Liu, Y., Wang, Y., Li, B., and Liu, J., Evaluation of the Performance of an Improved Solar Air Heater with "S" Shaped Ribs with Gap, *Sol. Energy*, vol. **195**, pp. 89–101, 2020.

Wang, X., Lei, B., Bi, H., and Yu, T., A Simplified Method for Evaluating Thermal Performance of Unglazed Transpired Solar Collectors under Steady State, *Appl. Therm. Eng*., vol. **117**, pp. 185–192, 2017.

Yassien, H.N.S., Alomar, O.A., and Salih, M.M.M., Performance Analysis of Triple-Pass Solar Air Heater System: Effects of Adding a Net of Tubes below Absorber Surface, *Sol. Energy*, vol. **207**, pp. 813–824, 2020.

Yu, D., Duan, H., Song, Q., Li, X., Zhang, H., Zhang, H., Liu, Y., Shen, W., and Wanh J., Characterizing the Environmental Impact of Metals in Construction and Demolition Waste, *Environ. Sci. Pollution Res*., vol. **25**, pp. 13823–13832, 2018.

Zare, D., Minaei, S., Mohamad-Zadeh, M., and Khoshtaghaza, M.H., Computer Simulation of Rough Rice Drying in a Batch Dryer, *Energy Convers. Manage*., vol. **47**, pp. 3241–3254, 2006.

Zhang, R., Ma, X., Shen, X., Zhai, Y., Zhang, T., Ji, C., and Hong, J., PET Bottles Recycling in China: An LCA Coupled with LCC Case Study of Blanket Production Made of Waste PET Bottles, *J. Environ. Manage.*, vol. **260**, p. 110062, 2020.

Zhou, Z., Chi, Y., Dong, J., Tang, Y., and Ni, M., Model Development of Sustainability Assessment from a Life Cycle Perspective: A Case Study on Waste Management Systems in China, *J. Clean. Prod.*, vol. **210**, pp. 1005–1014, 2019.